

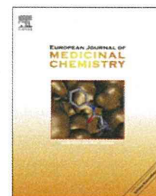
- therapy in genotype 1 chronic hepatitis C using data mining analysis. *J Gastroenterol* 2011; 46: 401–9.
- 13 McHutchison JG, Manns M, Patel K *et al.* Adherence to combination therapy enhances sustained response in genotype-1-infected patients with chronic hepatitis C. *Gastroenterology* 2002; 123: 1061–9.
 - 14 Ito K, Higami K, Masaki N *et al.* The rs8099917 polymorphism, when determined by a suitable genotyping method, is a better predictor for response to pegylated alpha interferon/ribavirin therapy in Japanese patients than other single nucleotide polymorphisms associated with interleukin-28B. *J Clin Microbiol* 2011; 49: 1853–60.
 - 15 Lyamichev V, Mast AL, Hall JG *et al.* Polymorphism identification and quantitative detection of genomic DNA by invasive cleavage of oligonucleotide probes. *Nat Biotechnol* 1999; 17: 292–6.
 - 16 Lyamichev VI, Kaiser MW, Lyamicheva NE *et al.* Experimental and theoretical analysis of the invasive signal amplification reaction. *Biochemistry* 2000; 39: 9523–32.
 - 17 Akuta N, Suzuki F, Hirakawa M *et al.* Amino acid substitution in hepatitis C virus core region and genetic variation near the interleukin 28B gene predict viral response to telaprevir with peginterferon and ribavirin. *Hepatology* 2010; 52: 421–9.
 - 18 Rauch A, Kutalik Z, Descombes P *et al.* Genetic variation in IL28B is associated with chronic hepatitis C and treatment failure: a genome-wide association study. *Gastroenterology* 2010; 138: 1338–45. 45 e1–7.
 - 19 Montes-Cano MA, Garcia-Lozano JR, Abad-Molina C *et al.* Interleukin-28B genetic variants and hepatitis virus infection by different viral genotypes. *Hepatology* 2010; 52: 33–7.
 - 20 Yamada G, Iino S, Okuno T *et al.* Virological response in patients with hepatitis C virus genotype 1b and a high viral load: impact of peginterferon-alpha-2a plus ribavirin dose reductions and host-related factors. *Clin Drug Investig* 2008; 28: 9–16.
 - 21 Bourliere M, Ouzan D, Rosenheim M *et al.* Pegylated interferon-alpha2a plus ribavirin for chronic hepatitis C in a real-life setting: the Hepatys French cohort (2003–2007). *Antivir Ther* 2012; 17: 101–10.
 - 22 Karasu Z, Tekin F, Ersoz G *et al.* Liver fibrosis is associated with decreased peripheral platelet count in patients with chronic hepatitis B and C. *Dig Dis Sci* 2007; 52: 1535–9.
 - 23 Everson GT, Hoefs JC, Seeff LB *et al.* Impact of disease severity on outcome of antiviral therapy for chronic hepatitis C: lessons from the HALT-C trial. *Hepatology* 2006; 44: 1675–84.
 - 24 Suzuki MM, Bird A. DNA methylation landscapes: provocative insights from epigenomics. *Nat Rev Genet* 2008; 9: 465–76.
 - 25 Boks MP, Derks EM, Weisenberger DJ *et al.* The relationship of DNA methylation with age, gender and genotype in twins and healthy controls. *PLoS ONE* 2009; 4: e6767.
 - 26 Li JH, Lao XQ, Tillmann HL *et al.* Interferon-lambda genotype and low serum low-density lipoprotein cholesterol levels in patients with chronic hepatitis C infection. *Hepatology* 2010; 51: 1904–11.
 - 27 Gopal K, Johnson TC, Gopal S *et al.* Correlation between beta-lipoprotein levels and outcome of hepatitis C treatment. *Hepatology* 2006; 44: 335–40.
 - 28 Toyoda H, Kumada T. Cholesterol and lipoprotein levels as predictors of response to interferon for hepatitis C. *Ann Intern Med* 2000; 133: 921.



ELSEVIER

Contents lists available at SciVerse ScienceDirect

European Journal of Medicinal Chemistry

journal homepage: <http://www.elsevier.com/locate/ejmech>

Original article

Inhibition of hepatitis C virus NS5B polymerase by S-trityl-L-cysteine derivatives

Daniel B. Nichols^a, Guy Fournet^b, K.R. Gurukumar^a, Amartya Basu^a, Jin-Ching Lee^c, Naoya Sakamoto^d, Frank Kozielski^e, Ira Musmuca^f, Benoît Joseph^{b,**}, Rino Ragno^{f,***}, Neerja Kaushik-Basu^{a,*}^a Department of Biochemistry and Molecular Biology, UMDNJ-New Jersey Medical School, 185 South Orange Avenue, Newark, NJ 07103, USA^b Institut de Chimie et Biochimie Moléculaires et Supramoléculaires, UMR-CNRS 5246, Université de Lyon, Université Claude Bernard – Lyon 1, Bâtiment Curien, 43 Boulevard du 11 Novembre 1918, F-69622 Villeurbanne, France^c Department of Biotechnology, College of Life Science, Kaohsiung Medical University, Kaohsiung, Taiwan^d Department of Gastroenterology and Hepatology, Tokyo Medical and Dental University, Tokyo 113-8519, Japan^e The Beatson Institute for Cancer Research, Molecular Motors Laboratory, Garscube Estate, Switchback Road, Bearsden, Glasgow G61 1BD, UK^f Rome Center for Molecular Design, Dipartimento di Chimica e Tecnologia del Farmaco, Sapienza Università di Roma, P.le A. Moro 5, 00185 Rome, Italy

ARTICLE INFO

Article history:

Received 20 December 2011

Received in revised form

3 January 2012

Accepted 5 January 2012

Available online 12 January 2012

Keywords:

Antiviral agents

Hepatitis C

HCV NS5B polymerase

Inhibitors

STLC derivatives

ABSTRACT

Structure-based studies led to the identification of a constrained derivative of S-trityl-L-cysteine (STLC) scaffold as a candidate inhibitor of hepatitis C virus (HCV) NS5B polymerase. A panel of STLC derivatives were synthesized and investigated for their activity against HCV NS5B. Three STLC derivatives, **9**, F-3070, and F-3065, were identified as modest HCV NS5B inhibitors with IC₅₀ values between 22.3 and 39.7 μM. F-3070 and F-3065 displayed potent inhibition of intracellular NS5B activity in the BHK-NS5B-FRLuc reporter and also inhibited HCV RNA replication in the Huh7/Rep-Feo1b reporter system. Binding mode investigations suggested that the STLC scaffold can be used to develop new NS5B inhibitors by further chemical modification at one of the trityl phenyl group.

© 2012 Elsevier Masson SAS. All rights reserved.

1. Introduction

Hepatitis C virus (HCV) infection represents a major public-health concern. It is estimated that over 200 million people, ~3% of the world population, are chronically infected with the virus [1–3]. HCV has an array of immune evasion strategies and can persist in the host for years. Individuals with chronic HCV infection are at increased risk of developing cirrhosis and hepatocellular carcinoma [3–7]. Currently, HCV infections are treated by a combination of pegylated-interferon, the nucleoside analog ribavirin, and one of two recently approved HCV protease inhibitors, Boceprevir or Telaprevir [8–13]. However, this therapy is limited in efficacy against the various HCV genotypes. Furthermore, in addition to its high cost, the current treatment is associated with severe side effects and a complicated dosing regimen that may limit patient compliance [11,12]. Also the possibility of selecting drug resistant HCV variants remains [12,13]. Therefore, the development

of additional, efficacious and more cost effective HCV antiviral therapies that target viral proteins and have limited effects on host biological processes is a priority.

HCV is a member of the *Flaviviridae* family. The positive sense, 9.6 kb RNA genome is translated into a single 3000 amino acid polyprotein via an IRES sequence located within the 5' non-translated region (NTR) of the viral genome [14,15]. The viral polyprotein is processed by both host and viral proteases into individual viral proteins consisting of four structural (core, E1, E2, and p7) and six nonstructural proteins (NS2, NS3, NS4A, NS4B, NS5A, and NS5B) [16]. HCV replicates exclusively in the cytoplasm of host cells. Replication of the viral RNA genome is mediated by the RNA-dependent RNA polymerase (RdRp) activity of the HCV nonstructural protein NS5B [17–19]. Because of the absolute requirement of NS5B to synthesize nascent HCV RNA, NS5B represents an attractive target for the development of anti-HCV inhibitors [20,21]. Furthermore, host cells lack RdRp. Therefore, an inhibitor that blocks RdRp activity should, in theory, have minimal or no effect on host biological processes. Though, a number of NIs and NNIs with potent in vitro anti-NS5B activity have been identified in recent years, they have presented challenges of toxicity and selection of resistant viruses, thus necessitating identification of better NS5B inhibitor scaffolds.

* Corresponding author. Tel.: +1 973 972 8653; fax: +1 973 972 5594.

** Corresponding author. Tel.: +33 4 72448135; fax: +33 4 72431214.

*** Corresponding author. Tel.: +396 4991 3937; fax: +396 4991 3627.

E-mail addresses: benoit.joseph@univ-lyon1.fr (B. Joseph), rino.ragno@uniroma1.it (R. Ragno), kaushik@umdnj.edu (N. Kaushik-Basu).

The structure of NS5B has been extensively characterized. The 66 kDa viral polymerase resembles a “right hand” with the active site contained in the palm domain and the RNA interacting region in the finger and thumb domains [22–25]. Current NS5B inhibitors can be divided into two classes, nucleoside inhibitors (NI) and non-nucleoside inhibitors (NNI). Once converted by host proteins into nucleotides, NIs cause RNA-chain termination upon incorporation by NS5B into the nascent RNA chains. NNIs bind to one of the five allosteric sites on NS5B and inhibit the initiation step of RNA synthesis.

Recently, we reported on the utility of three-dimensional quantitative structure-activity relationship (3D-QSAR) in combination with ligand-based and structure-based alignment procedures for *in silico* screening of new HCV NS5B polymerase inhibitors [26]. This investigation identified four new NS5B inhibitors from forty candidates examined from the NCI diversity set [26]. The most interesting hit, NSC123526 (Fig. 1), has been reported to be active against other viruses [27] and can be simply viewed as a constrained derivative of the S-trityl-L-cysteine (STLC) scaffold. STLC derivatives are versatile compounds endowed with antileukemic activity [28] and are also reported to inhibit the human mitotic kinesin Eg5 (HMKEg) by a non-competitive mechanism [29].

Herein, we describe molecular modeling studies that led us to explore the potential of STLC and its derivatives to inhibit HCV NS5B RdRp activity *in vitro*. Further, we examined the effect of STLC derivatives on intracellular HCV NS5B RdRp activity and on HCV RNA replication. Among the tested STLC derivatives, we identified three compounds as novel HCV NS5B inhibitor leads. These compounds merit further optimization through classical medicinal chemistry and virtual screening.

2. Results and discussion

2.1. Molecular modeling

Recently, we utilized structure-based 3-D QSAR modeling to identify NS5B thumb-binding inhibitors and reported on the identification of NSC123526 as a modest HCV NS5B inhibitor [26]. NSC123526 can be considered as a constrained STLC derivative (Fig. 1). Since STLC derivative NSC123139 (Fig. 1) was found to be most potent in inhibiting HMKEg, we performed cross-docking experiments to investigate whether it could also bind the HCV-NS5B thumb domain [26,29]. Fig. 2 depicts the docked conformation of NSC123139 in HCV-NS5B and HMKEg.

The activity of the docked NSC123139 (Predicted pIC_{50} = 5.64) was predicted by our 3-D QSAR model in the same range of NSC123526 (Experimental pIC_{50} = 4.33, predicted pIC_{50} = 5.4) [26]. However, NSC123139 exhibited a much weaker inhibition of NS5B RdRp activity *in vitro* (Table 1), compared to NSC123526, as previously reported [26].

Based on the above partial results, we tested a series of STLC derivatives for their ability to inhibit NS5B, with the objective of identifying new lead scaffolds. While our investigations with additional STLC derivatives were still ongoing, the co-crystal structures of HMKEg with NSC123139 (pdb entry code 2wog and 2xae) and other STLCs (2xr2 and 3ken) were released [30]. Nevertheless, docking calculations performed through Autodock Vina, were in good agreement with the experimental results (rmsd = 0.44) and with similar docking calculations previously reported [31], thus supporting our protocol.

The above docking protocol was also applied to the other STLCs. In addition, we analyzed the Autodock Vina proposed binding

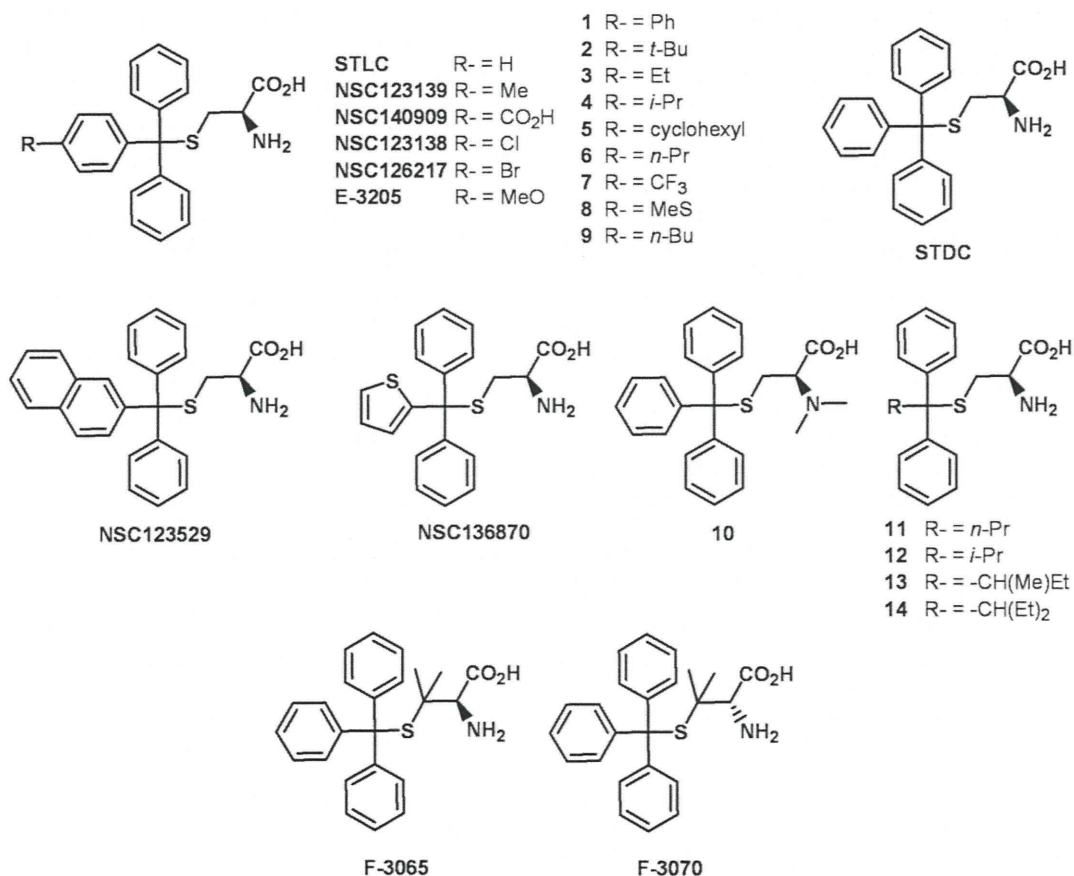


Fig. 1. Structures of NSC123526, STLC, STDC and STLC derivatives.

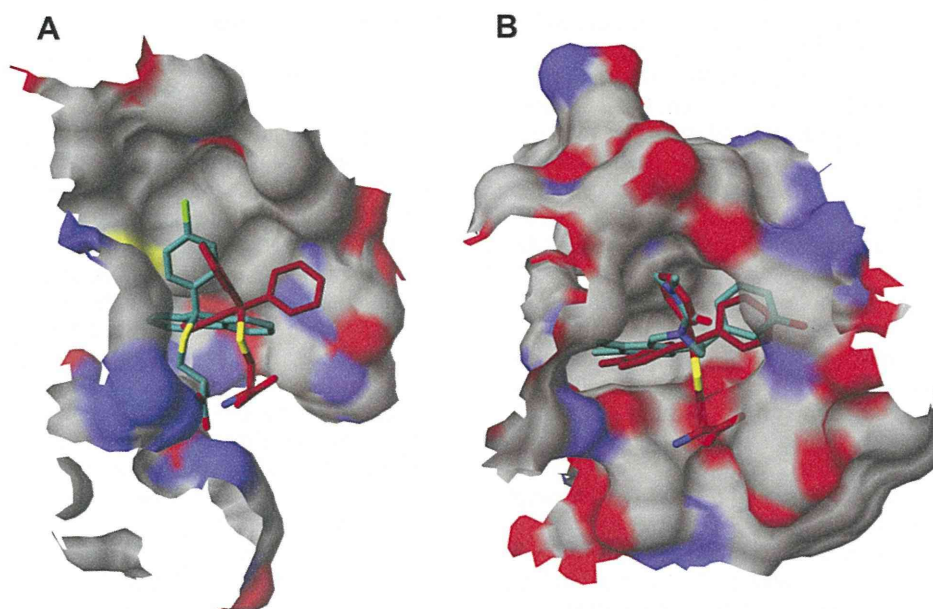


Fig. 2. Molecular docking of STL derivatives in NS5B. Panel A: Docked conformations of NSC123139 (red-colored carbon atoms) and NSC123526 (green-colored carbon atoms) within NS5B thumb domain. Panel B: HMKeg (PDB entry code 2fme) with docked conformation of NSC123139 (red-colored carbon atoms) and the experimental bound NSC123526 (green-colored carbon atoms). (For interpretation of the references to colour in this figure legend, the reader is referred to the web version of this article.)

mode of the two most active compounds, F-3065 and F-3070, cross-docked into the 15 NS5B-NNI co-crystal structures as previously described by us [26]. As expected, docked conformations of F-3065 and F-3070 ((*R*) and (*S*) enantiomers of the same compound, respectively) exhibited the lowest binding energy in the PDB entry 2d3u. Further, the bound conformations of F-3065 and F-3070, in agreement with the biological data, revealed that the cysteine stereocenter does not affect the overall binding mode, wherein the terminal amino acid group is involved in a hydrogen bonding network, as shown in the ligplot diagrams in Fig. 3. In particular the α -amino acid portion of F-3065 makes two hydrogen bonds, one between its amino group and the carbonyl group of Trp528 ($N\cdots O$ distance = 3.01 Å) and the other between a carboxy oxygen and the ϵ -amino group of Lys533 ($O\cdots N$ distance = 2.98 Å) (Fig. 3A). The ligplot diagram of the (*S*) enantiomer F-3070, that forms two hydrogen bonds with its two carboxy oxygens, one with the guanidinic nitrogen of Arg501 ($O\cdots N$ distance = 3.21 Å) and the other with ϵ -amino group of Lys533 ($O\cdots N$ distance 3.05–3.22 Å), is shown in Fig. 3B. This type of hydrogen bonding network was observed in all other STL derivatives (Fig. 5) suggesting that hydrogen bonds are the leading interactions.

Other notable interactions are hydrophobic in nature, and the trityl moieties are buried in the thumb allosteric binding side (Fig. 4). For both F-3065 and F-3070, one phenyl is placed in a pocket formed by Leu419, Arg422, Met423 and Trp528, while the other two benzenes fill-up two depressions on the enzyme surface. By comparing the binding mode of the most active STLs with that of the experimental co-crystallized compound found in 2d3u and considering the conserved binding modes shown in Fig. 5, we believe the STL can be used as a starting scaffold, whose activity could be improved by inserting a side chain in one of the two surface bound benzene rings to better fill the binding cleft formed by Leu419, Met423, Ile482, Val485, Ala486, Leu489 and Leu497 (Fig. 6) and occupied by a 2-(4-cyanophenyl)thiophene group in the original complex (PDB ID 2d3u). As expected and within the limit of any predictive model, the application of our 3-D QSAR to all the new STLs, predicted these compounds to have activities between the 10–100 μM range (data not shown).

2.2. Chemistry

A total of 35 STL derivatives were utilized in this study (Fig. 1 and Scheme 1). STL and 14 derivatives (**1–14**) have been reported previously [29,31]. Compounds F-3070 and F-3065 were purchased from Bachem, while STDC (NSC123676), NSC123139, NSC136870, NSC140909, NSC123529, NSC123138, and NSC126217 were procured from NCI/NIH. In accordance with published literature, 12 STL derivatives were newly synthesized for this investigation (Scheme 1). Starting aryldiphenylmethanol compounds **15** were prepared in good yields from appropriate esters (ArCO_2Me) and phenylmagnesium chloride (data not shown) [32]. Condensation of cysteamine.HCl (**16**) with $\text{Ar}(\text{Ph})_2\text{COH}$ ($\text{Ar} = 4\text{-Me-Ph}$, 4-Et-Ph , $4\text{-}n\text{-Pr-Ph}$, 4-MeS-Ph , 4-I-Ph , 4-(Ph)-Ph and 2-naphthyl) **15a–g** in TFA gave final compounds **17a–g** in 29–47% yield (Scheme 1). Treatment of *L*-cysteine (**18**) or *L*-penicillamine (**19**) with $\text{Ar}(\text{Ph})_2\text{COH}$ ($\text{Ar} = 4\text{-(}n\text{-C}_5\text{H}_{11}\text{)-Ph}$, $4\text{-(}n\text{-C}_6\text{H}_{13}\text{)-Ph}$, 4-PrO-Ph and $4\text{-}n\text{-Bu-Ph}$) **15h–k** in the presence of $\text{BF}_3 \cdot \text{Et}_2\text{O}$ afforded target compounds **17h–i** in 30–55% yield (Scheme 1).

2.3. Biological studies

With the objective of identifying novel HCV NS5B inhibitors, we investigated STL and its derivatives employing the *in vitro* NS5B RdRp inhibition assay as described previously [33–35]. Recombinant HCV NS5B (genotype 1b) carrying an N-terminal His-tag and C-terminal 21-amino acid truncation (NS5BC Δ 21) was purified to homogeneity by Ni-NTA chromatography and used as a source of enzyme [33–35]. Wedelolactone, a documented NS5B inhibitor, was employed as an internal reference standard, and yielded an IC_{50} value of 36.0 μM (data not shown), consistent with our previously reported value [34]. In order to identify a wider range of NS5B inhibitor candidates, preliminary screening of STL and its derivatives was conducted at 100 μM compound concentration. While the parent STL molecule yielded only $\sim 12\%$ inhibition of NS5B RdRp activity during preliminary screening, its thirty-five derivatives, with the exception of **17i**, exhibited a much higher inhibition ranging from 14 to 83% (Table 1). Of these, three compounds **9**, F-

Table 1
Anti-HCV NS5B RdRp activity of STLC derivatives.

Compound	% Inhibition ^a	IC ₅₀ (μM) ^b
STLC	12.6 ± 2.3	n.d.
STDC	17.0 ± 0.6	n.d.
NSC123139	23.1 ± 1.6	n.d.
NSC136870	23.4 ± 2.9	n.d.
NSC140909	30.9 ± 3.7	n.d.
NSC123529	14.7 ± 1.5	n.d.
NSC123138	28.3 ± 5.9	n.d.
NSC126217	20.2 ± 2.5	n.d.
1	22.4 ± 5.4	n.d.
2	22.6 ± 2.0	n.d.
3	36.8 ± 2.4	n.d.
4	31.2 ± 1.5	n.d.
5	20.5 ± 1.1	n.d.
6	36.9 ± 2.5	n.d.
7	43.5 ± 0.8	n.d.
8	44.3 ± 3.0	n.d.
9	60.0 ± 3.4	39.7 ± 0.9
10	17.2 ± 2.9	n.d.
11	19.1 ± 1.7	n.d.
12	22.5 ± 2.2	n.d.
13	34.0 ± 1.1	n.d.
14	33.1 ± 0.7	n.d.
17a	31.7 ± 1.8	n.d.
17b	28.7 ± 2.1	n.d.
17c	27.4 ± 4.2	n.d.
17d	24.0 ± 4.5	n.d.
17e	36.7 ± 2.1	n.d.
17f	36.0 ± 1.0	n.d.
17g	33.3 ± 2.3	n.d.
17h	28.3 ± 5.9	n.d.
17i	16.1 ± 3.0	n.d.
17j	14.0 ± 3.3	n.d.
17k	22.0 ± 1.4	n.d.
17l	n.i.	n.d.
F-3070	82.8 ± 1.3	22.3 ± 5.9
E-3205	40.2 ± 0.7	n.d.
F-3065	76.7 ± 2.4	24.6 ± 6.0

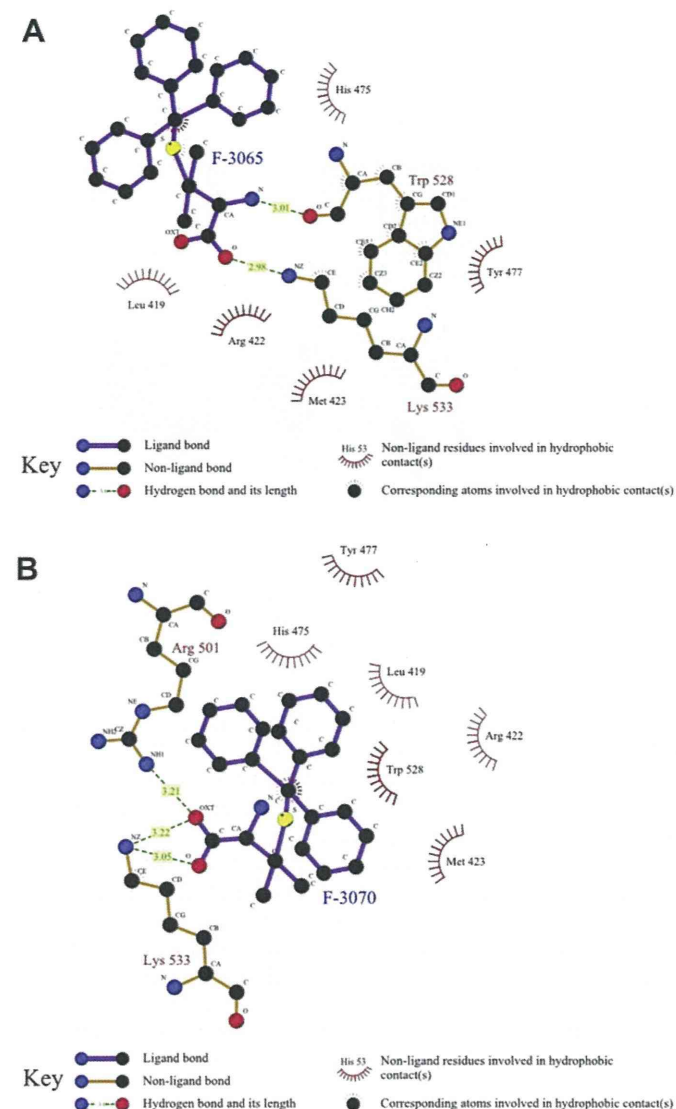
n.d., not determined.

n.i., no inhibition.

^a Percent inhibition was determined at 100 μM concentration of the indicated compound and represents an average of at least two independent measurements in duplicate.^b The IC₅₀ values of the compounds were determined from dose-response curves employing 8–12 concentrations of each compound in duplicate in two independent experiments. Curves were fitted to data points using nonlinear regression analysis and IC₅₀ values were interpolated from the resulting curves using GraphPad Prism 3.03 software.

3070, and F-3065 having ≥60% anti-NS5B activity at 100 μM were further pursued for their IC₅₀ value determination. This analysis resulted in the identification of F-3070 and F-3065 with near similar IC₅₀ values, as the two most potent of the 36 STLC derivatives examined in this investigation, while **9** exhibited ~1.6–1.8-fold higher IC₅₀ value compared to the two afore-mentioned compounds. Together, these data suggest that STLC scaffold may offer further scope for improvement of its anti-NS5B activity.

To evaluate the anti-HCV activity of STLC compounds in a more biologically relevant setting, we employed the BHK-NS5B-FRLuc reporter and the Huh7/Rep-Feo1b reporter systems [36,37]. The former reporter system carries stably transfected NS5B and a bicistronic reporter gene, (+)FLuc(-)UTR-RLuc for cell based investigations of HCV NS5B RdRp inhibitors [36]. The advantage of this system is that it can simultaneously measure intracellular HCV NS5B RdRp activity as reflected by the ratio of *Renilla* to firefly luciferase luminescence and cellular viability which is reflected by the firefly luciferase luminescence, thus enabling the identification of potent non-toxic inhibitors. The Huh7/Rep-Feo1b reporter system, on the other hand, autonomously replicates the subgenomic HCV genotype 1b replicon RNA carrying the firefly luciferase

**Fig. 3.** Panel A: Ligplot diagram for F-3065 docked in NS5B (PDB ID 2d3u). Panel B: Ligplot diagram for F-3070 docked in NS5B (PDB ID 2d3u).

reporter as an indicator of HCV RNA replication, and has been widely employed to identify inhibitors of HCV RNA replication [37].

Only three STLC derivatives F-3070, F-3065, and E-3205 inhibited intracellular NS5B RdRp activity in the BHK-NS5B-FRLuc reporter at 100 μM concentration (Table 2). The two more potent of these, F-3070 and F-3065 exhibited ≥84% inhibition while E-3205 displayed only ~44% inhibition of NS5B RdRp activity, consistent with the in vitro data. In terms of their cytotoxicity parameters, F-3070 and F-3065 did not affect cell viability at 100 μM, as was evident from equivalent levels of firefly luciferase luminescence in compound treated cells versus DMSO controls. Treatment with E-3205 however, decreased cell viability by ~70% at 100 μM concentration. The remaining thirty-three STLC derivatives as well as the parent molecule, exhibited ≥50% reduction in cell viability at 100 μM, with only a marginal 15–30% decrease in intracellular NS5B activity (data not shown), consistent with the in vitro RdRp data.

In the Huh7/Rep-Feo1b reporter system, compounds F-3070 and F-3065 exhibited an overall similar pattern of cell viability and HCV RNA replication inhibition, corresponding to ~73–74% and ~89–91%, respectively at 100 μM concentration (Table 2). E-3205,

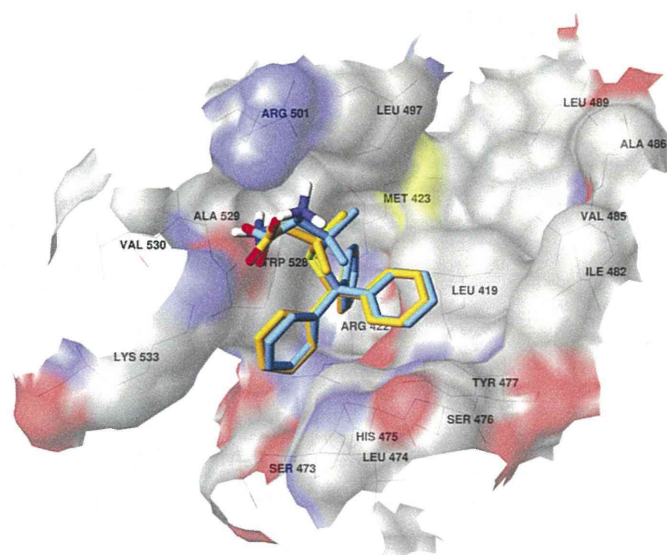


Fig. 4. Docked conformation of F-3065 (orange) and F-3070 (cyan) in NS5B (PDB ID 2d3u). The enzyme surface is shown in atom type color. (For interpretation of the references to colour in this figure legend, the reader is referred to the web version of this article.)

however, exhibited decreased cell viability (44%) compared to the other two compounds, though its inhibition of HCV RNA replication (~89%) was similar. It is worth noting here that the inhibition observed in this system may be partly attributed to the cellular toxicity effects of these compounds.

The results in this present study suggest that STLC derivatives inhibit HCV RNA replication by targeting the NS5B polymerase. It is possible that other host factors such as HMKEg are also targeted by STLCs in the HCV replicase complex and needs to be elucidated. These studies provide a platform to optimize the STLC scaffold as a potent anti-NS5B inhibitor. An extensive focused virtual screening approach is ongoing on a database constituted of more than 500 K trityl cysteine analogs to optimize the newly reported lead compounds.

3. Conclusion

In summary, STLC derivatives were identified as novel inhibitors of HCV NS5B polymerase activity in vitro and in cell based assays.

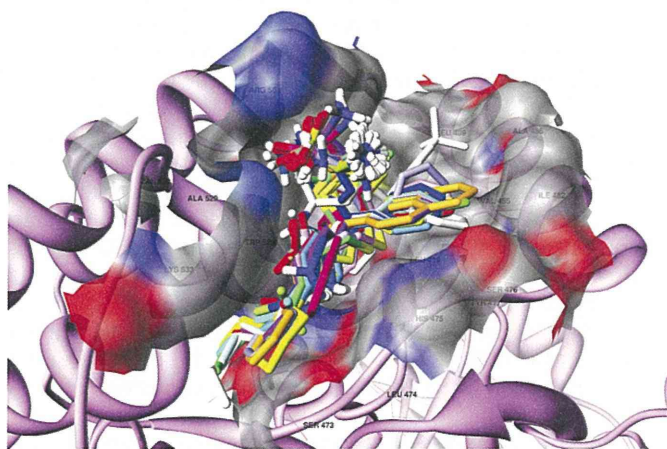


Fig. 5. STLC analogues docked within the HCV NS5B (in pink ribbon) thumb allosteric surface. The compounds overlap in this pocket. (For interpretation of the references to colour in this figure legend, the reader is referred to the web version of this article.)

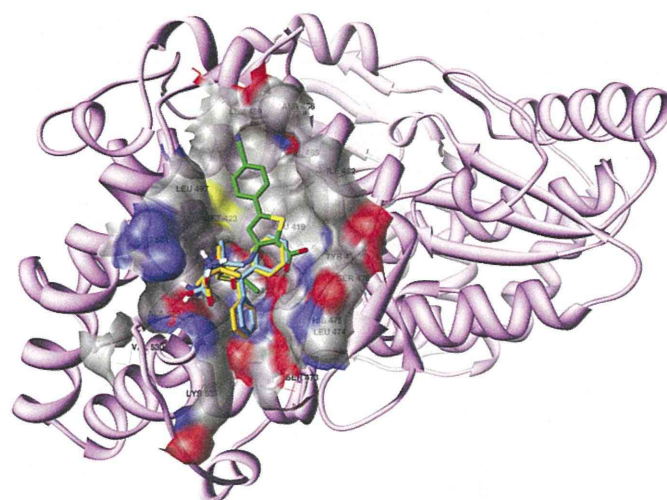


Fig. 6. F-3065 (orange) and F-3070 (cyan) overlapped on the 2d3u co-crystallized ligand (green). HCV NS5B (PDB ID 2d3u, in pink ribbon) and the thumb allosteric surface (in atom type color) are also shown. (For interpretation of the references to colour in this figure legend, the reader is referred to the web version of this article.)

This study validates structure-based molecular modeling coupled with 3-D QSAR prediction, as a viable strategy for identification of new structural scaffolds targeting NS5B. STLC binding mode analysis revealed a common way by which STLCs bind to the HCV NS5B thumb allosteric site and further suggested that improved STLC derivatives may be achieved by chemical modification at one of the trityl phenyl ring.

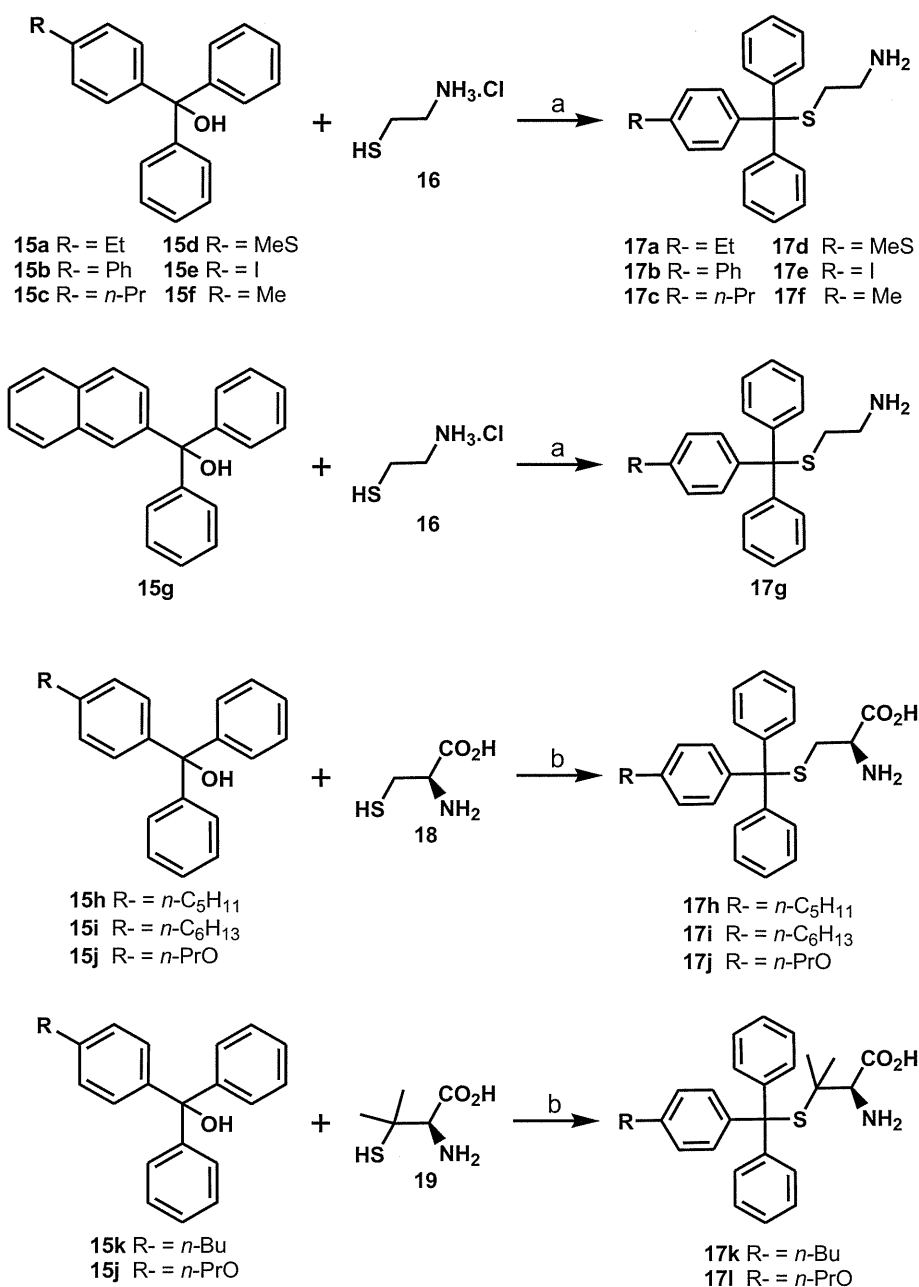
4. Experimental section

4.1. Molecular modeling

All molecules were generated by means of molecular mechanics of Chemaxon Marvin software (<http://www.chemaxon.com/>). Molecular graphics images were produced using UCSF Chimera package from the Resource for Biocomputing, Visualization, and Informatics at the University of California, San Francisco on a 3 GHz AMD CPU equipped IBM-compatible workstation with the Debian 5.0 version of the Linux operating system. Different from the previous protocol, the faster Autodock Vina [38] docking program was used in place of Autodock for all docking studies. Docking assessment was conducted via re-docking, re-docking modeled, cross-docking and cross-docking modeled as previously reported [26]. Autodock Vina proved to be as good as Autodock (data not shown), but much faster in calculations. The compounds were then submitted for structure-based molecular alignment through cross-docking protocols as previously reported [26]. For activity predictions, the previously developed SB 3-D QSAR model was applied without any modification [26]. The program ligplot v. 4.0 was used [39] to generate the ligand/NS5B interaction maps.

4.2. Chemistry

General methods: Melting points were determined using a Büchi capillary instrument and are uncorrected. Optical rotations were measured at the sodium D line (589 nm) at 25 °C with a Perkin–Elmer 241 polarimeter using a 1 dm path length cell. ^1H and ^{13}C NMR spectra were recorded on a Bruker 300, 400 or 500 MHz spectrometers. Chemical shifts (δ) are in parts per million. The following abbreviations were used to designate the multiplicities: s = singlet, d = doublet, t = triplet, q = quartet, m = multiplet, br = broad. Mass spectra were recorded with a Perkin–Elmer SCIEX



Scheme 1. Synthesis of STLC derivatives **17a–l**. Reagents and conditions: (a) TFA, rt, 3 h; (b) BF₃·Et₂O, AcOH, rt, 2 h.

API spectrometer. Elemental analyses were performed on a Thermoquest Flash 1112 series EA analyzer. Elemental analyses were found to be within ± 0.4 of the theoretical values. Purity of tested compounds was $>95\%$. All commercially available reagents and solvents were used without further purification. STLC and derivatives **1–14** have been previously described [29]. E-3205, F-3070 and F-3065 were purchased from Bachem. STDC (NSC124676), NSC123139, NSC136870, NSC140909, NSC123529, NSC123138, and NSC126217 were procured from NCI/NIH.

4.2.1. General procedure for preparation of compounds **17a–g**

At 0 °C and under argon atmosphere, a solution of cysteamine HCl (**16**) (1.33 mmol) was added dropwise to a solution of appropriate alcohol **15** (1.33 mmol) in TFA (5 mL). The reaction mixture was stirred at room temperature for 1 h, evaporated and extracted with a saturated solution of NaHCO₃(aq) and EtOAc. The organic

Table 2
Anti-HCV effects of STLC derivatives in cell based reporter assay.

Compound	BHK-NS5B-FR Luc ^a		Huh7/Rep-Feo1b ^b	
	Viability (%)	Inhibition (%)	Viability (%)	Inhibition (%)
F-3070	100.0	85.4	72.6	89.5
E-3205	30.2	44.4	44.2	88.6
F-3065	100.0	84.3	74.1	91.2

^aBHK-NS5B-FRLuc and ^bHuh7/Rep-Feo1b reporter cells were treated with the indicated compounds at 100 μ M concentration for 42 h. Cell viability in the BHK-NS5B-FRLuc reporter^a was estimated as the relative levels of Firefly luciferase in compound treated cells versus DMSO controls, while that in the Huh7/Rep-Feo1b cells^b was evaluated by the MTS assay. The inhibitory effect of the compounds on NS5B RdRp activity^a and HCV RNA replication^b is presented as percent of DMSO treated controls. Data represents an average of three independent experiments in duplicate.

phase was dried over MgSO₄, filtered, and evaporated under vacuum. The oil was crystallized from Et₂O or Et₂O/pentane 1:1. The desired compounds **17a–g** were obtained by filtration in the range of 29–47% yield.

4.2.1.1. 2-[1-(4-Ethylphenyl)-1,1-diphenylmethylthio]jethanamine

(**17a**). Starting alcohol = 1-(4-ethylphenyl)-1,1-diphenylmethanol (**15a**). Yield: 31%; mp 138–140 °C; ¹H NMR (300 MHz, CD₃OD + D₂O): δ 1.23 (t, 3H, J = 7.5 Hz, CH₃), 2.45–2.59 (m, 4H, 2 CH₂), 2.58 (q, 2H, J = 7.5 Hz, CH₂), 7.17 (d, 2H, J = 8.5 Hz, H_{Ar}), 7.22–7.35 (m, 8H, H_{Ar}), 7.43–7.46 (m, 4H, H_{Ar}); ¹³C NMR (100 MHz, DMSO-*d*₆): δ 15.3 (CH₃), 27.6 (CH₂), 28.6 (CH₂), 37.7 (CH₂), 66.2 (Cq), 126.9 (2× CH), 127.5 (2× CH), 128.2 (4× CH), 129.0 (6× CH), 141.3 (Cq), 142.3 (Cq), 144.2 (2× Cq); MS (ESI): *m/z* 370 [M + Na]⁺; Anal. Calcd for C₂₃H₂₅NS: C 79.49, H 7.25, N 4.03, found: C, 79.47, H 7.20, N 3.97.

4.2.1.2. 2-[1,1-Diphenyl-4-(phenyl)phenylmethylthio]jethanamine

(**17b**). Starting alcohol = 1-(4-phenylphenyl)-1,1-diphenylmethanol (**15b**). Yield: 30%; mp 160–162 °C; ¹H NMR (300 MHz, CD₃OD + D₂O): δ 2.50–2.62 (s, 4H, 2 CH₂), 7.27–7.63 (m, 19H, H_{Ar}); ¹³C NMR (125 MHz, DMSO-*d*₆): δ 28.7 (CH₂), 37.8 (CH₂), 66.2 (Cq), 126.4 (2× CH), 126.6 (2× CH), 127.0 (2× CH), 127.6 (CH), 128.3 (4× CH), 128.9 (2× CH), 129.0 (4× CH), 129.6 (2× CH), 138.6 (Cq), 139.2 (Cq), 143.2 (Cq), 143.9 (2× Cq); MS (ESI): *m/z* 418 [M + Na]⁺; Anal. Calcd for C₂₇H₂₅NS: C 81.98, H 6.37; N 3.54, found: C 82.26, H 6.44, N 3.73.

4.2.1.3. 2-[1,1-Diphenyl-4-(propyl)phenylmethylthio]jethanamine

(**17c**). Starting alcohol = 1,1-diphenyl-1-(4-propylphenyl) methanol (**15c**). Yield: 45%; mp 133–135 °C; ¹H NMR (300 MHz, CD₃OD + D₂O): δ 0.94 (t, 3H, J = 7.3 Hz, CH₃), 1.58–1.70 (m, 2H, CH₂), 2.45–2.49 (m, 2H, CH₂), 2.50–2.60 (m, 4H, CH₂), 7.14 (d, 2H, J = 8.3 Hz, H_{Ar}), 7.22–7.34 (m, 8H, H_{Ar}), 7.42–7.45 (m, 4H, H_{Ar}); ¹³C NMR (100 MHz, DMSO-*d*₆): δ 13.8 (CH₃), 23.9 (CH₂), 28.6 (CH₂), 36.7 (CH₂), 37.7 (CH₂), 66.2 (Cq), 126.9 (2× CH), 128.1 (2× CH), 128.2 (4× CH), 128.9 (2× CH), 129.0 (4× CH), 140.8 (Cq), 141.3 (Cq), 144.2 (2× Cq); MS (ESI): *m/z* 384 [M + Na]⁺; Anal. Calcd for C₂₄H₂₇NS: C 79.73, H 7.53, N 3.87, found: C 79.55, H 7.40, N 3.82.

4.2.1.4. 2-[1,1-Diphenyl-4-(methylthio)phenylmethylthio]jethanamine

(**17d**). Starting alcohol = 1,1-diphenyl-1-(4-methylthiophenyl)methanol (**15d**). Yield: 40%; mp 142–144 °C; ¹H NMR (300 MHz, CD₃OD + D₂O): δ 2.47 (s, 3H, CH₃), 2.50–2.59 (m, 4H, CH₂), 7.20–7.37 (m, 10H, H_{Ar}), 7.43–7.46 (m, 4H, H_{Ar}); ¹³C NMR (125 MHz, DMSO-*d*₆): δ 14.3 (CH₃), 28.6 (CH₂), 37.7 (CH₂), 66.0 (Cq), 125.3 (2× CH), 127.0 (2× CH), 128.2 (4× CH), 128.9 (4× CH), 129.6 (2× CH), 137.0 (Cq), 140.3 (Cq), 143.9 (2× Cq); MS (ESI): *m/z* 388 [M + Na]⁺; Anal. Calcd for C₂₂H₂₃NS₂: C 72.28, H 6.34, N 3.83, found: C 72.00, H 6.35, N 3.77.

4.2.1.5. 2-[1-(4-Iodophenyl)-1,1-diphenylmethylthio]jethanamine

(**17e**). Starting alcohol = 1-(4-iodophenyl)-1,1-diphenylmethanol (**15e**). Yield: 47%; mp 150–152 °C; ¹H NMR (300 MHz, CD₃OD + D₂O): δ 2.54 (s, 4H, 2 CH₂), 7.21–7.36 (m, 8H, H_{Ar}), 7.41–7.44 (m, 4H, H_{Ar}), 7.68 (d, 2H, J = 10.8 Hz, H_{Ar}); ¹³C NMR (125 MHz, DMSO-*d*₆): δ 28.8 (CH₂), 37.7 (CH₂), 66.0 (Cq), 93.4 (Cq), 127.1 (2× CH), 128.3 (4× CH), 128.9 (4× CH), 131.4 (2× CH), 137.0 (2× CH), 143.5 (2× Cq), 143.8 (Cq); MS (ESI): *m/z* 468 [M + Na]⁺; Anal. Calcd for C₂₁H₂₀INS: C 56.63, H 4.53, N 3.15, found: C 56.60, H 4.61, N 3.22.

4.2.1.6. 2-[1-(4-Methylphenyl)-1,1-diphenylmethylthio]jethanamine

(**17f**). Starting alcohol = 1-(4-methylphenyl)-1,1-diphenylmethanol (**15f**). Yield: 29%; mp 138–140 °C; ¹H NMR (300 MHz, CD₃OD + D₂O): δ 2.32 (s, 3H, CH₃), 2.48–2.55 (m, 4H, 2 CH₂), 7.13 (d, 2H, J = 8.1 Hz,

H_{Ar}), 7.24–7.34 (m, 8H, H_{Ar}), 7.41–7.45 (m, 4H, H_{Ar}); ¹³C NMR (100 MHz, DMSO-*d*₆): δ 20.5 (CH₃), 29.0 (CH₂), 37.9 (CH₂), 66.2 (Cq), 126.9 (2× CH), 128.2 (4× CH), 128.7 (2× CH), 129.0 (6× CH), 136.1 (Cq), 141.1 (Cq), 144.2 (2× Cq); MS (ESI): *m/z* 356 [M + Na]⁺; Anal. Calcd for C₂₂H₂₃NS: C 79.23, H 6.95, N 4.20, found: C 78.88, H 7.03, N 4.19.

4.2.1.7. 2-[1-(2-Naphthyl)-1,1-(diphenyl)methylthio]jethanamine

(**17g**). Starting alcohol = 1-(2-naphthyl)-1,1-diphenylmethanol (**15g**) [32,40]. Yield: 32%; mp 126–128 °C; ¹H NMR (300 MHz, CD₃OD + D₂O): δ 2.34–2.47 (s, 4H, 2 CH₂), 7.21–7.34 (m, 6H, H_{Ar}), 7.43–7.49 (m, 6H, H_{Ar}), 7.55 (dd, 1H, J = 1.9, 8.9 Hz, H_{Ar}), 7.70–7.83 (m, 4H, H_{Ar}); ¹³C NMR (100 MHz, DMSO-*d*₆): δ 35.6 (CH₂), 40.8 (CH₂), 66.0 (Cq), 126.4 (CH), 126.5 (CH), 126.8 (2× CH), 127.2 (CH), 127.3 (CH), 127.5 (CH), 128.1 (5× CH), 128.2 (CH), 129.1 (4× CH), 131.6 (Cq), 132.3 (Cq), 141.9 (Cq), 144.5 (2× Cq); MS (ESI): *m/z* 392 [M + Na]⁺; Anal. Calcd for C₂₅H₂₃NS: C 81.26, H 6.27, N 3.79, found: C 81.38, H 6.31, N 3.89.

4.2.2. General procedure for preparation of compounds **17h–I**

At 0 °C and under argon atmosphere, a solution of BF₃·Et₂O (1.33 mmol) was added dropwise to a solution of appropriate alcohol **15** (0.86 mmol), L-cysteine (**18**) or L-penicillamine (**19**) (0.77 mmol) in AcOH (1 mL). The reaction mixture was stirred at room temperature for 3 h. Addition of 10% solution of NaOAc (2 mL), then H₂O (2 mL) led to the formation of a gum. After elimination of the supernatant, the final compound was precipitated by addition of pentane or Et₂O. The desired compounds **17h–I** were obtained by filtration in the range of 30–55% yield.

4.2.2.1. S-[1-(4-Pentylphenyl)-1,1-diphenylmethyl]-L-cysteine

(**17h**). Starting alcohol = 1-(4-pentylphenyl)-1,1-diphenylmethanol (**15h**). Yield: 55%; mp 127–129 °C; [α]_D²⁵ = +61 (c = 0.52 in MeOH); ¹H NMR (300 MHz, CD₃OD + D₂O): δ 0.91 (t, 3H, J = 6.7 Hz, CH₃), 1.32–1.39 (m, 4H, 2 CH₂), 1.56–1.66 (m, 2H, CH₂), 2.59 (broad t, 2H, J = 7.9 Hz, CH₂), 2.70 (dd, 1H, J = 9.2, 13.5 Hz, CH₂), 2.82 (dd, 1H, J = 4.2, 13.5 Hz, CH₂), 3.04 (dd, 1H, J = 4.2, 9.2 Hz, CH), 7.13 (d, 2H, J = 8.5 Hz, H_{Ar}), 7.20–7.35 (m, 8H, H_{Ar}), 7.43–7.46 (m, 4H, H_{Ar}); ¹³C NMR (100 MHz, CD₃OD): δ 14.4 (CH₃), 23.6 (CH₂), 32.3 (CH₂), 32.7 (CH₂), 34.0 (CH₂), 36.4 (CH₂), 54.6 (CH), 68.0 (Cq), 128.0 (2× CH), 129.1 (6× CH), 130.6 (2× CH), 130.7 (4× CH), 142.8 (Cq), 143.0 (Cq), 145.8 (2× Cq), 172.0 (CO); MS (ESI): *m/z* 456 [M + Na]⁺; Anal. Calcd for C₂₇H₃₁NO₂S: C 74.79, H 7.21, N 3.23, found: C 74.79, H 7.17, N 3.25.

4.2.2.2. S-[1-(4-Hexylphenyl)-1,1-diphenylmethyl]-L-cysteine

(**17i**). Starting alcohol = 1-(4-hexylphenyl)-1,1-diphenylmethanol (**15i**). Yield: 40%; mp 129–131 °C; [α]_D²⁵ = +53 (c = 0.54 in MeOH). ¹H NMR (300 MHz, CD₃OD + D₂O): δ 0.90 (t, 3H, J = 6.7 Hz, CH₃), 1.30–1.42 (m, 6H, 3 CH₂), 1.54–1.66 (m, 2H, CH₂), 2.59 (broad t, 2H, J = 7.9 Hz, CH₂), 2.70 (dd, 1H, J = 9.2, 13.5 Hz, CH₂), 2.82 (dd, 1H, J = 4.2, 13.5 Hz, CH₂), 3.03 (dd, 1H, J = 4.2, 9.2 Hz, CH), 7.12 (d, 2H, J = 8.3 Hz, H_{Ar}), 7.21–7.35 (m, 8H, H_{Ar}), 7.43–7.46 (m, 4H, H_{Ar}); ¹³C NMR (100 MHz, CD₃OD): δ 14.4 (CH₃), 23.7 (CH₂), 30.1 (CH₂), 32.5 (CH₂), 32.8 (CH₂), 34.0 (CH₂), 36.4 (CH₂), 54.7 (CH), 68.0 (Cq), 128.0 (2× CH), 129.1 (6× CH), 130.6 (2× CH), 130.7 (4× CH), 142.8 (Cq), 143.0 (Cq), 145.8 (2× Cq), 172.0 (CO); MS (ESI): *m/z* 470 [M + Na]⁺; Anal. Calcd for C₂₈H₃₃NO₂S: C 75.13, H 7.43, N 3.13, found: C 74.87, H 7.30, N 3.02.

4.2.2.3. S-[1,1-Diphenyl-1-(4-propoxyphenyl)methyl]-L-cysteine

(**17j**). Starting alcohol = 1,1-diphenyl-1-(4-propoxyphenyl)methanol (**15j**) [41]. Yield: 43%; mp 144–146 °C; [α]_D²⁵ = +60 (c = 0.51 in MeOH); ¹H NMR (300 MHz, CD₃OD + D₂O): δ 1.03 (t, 3H, J = 7.3 Hz, CH₃), 1.72–1.84 (m, 2H, CH₂), 2.68 (dd, 1H, J = 9.2, 13.4 Hz, CH₂), 2.83 (dd,

1H, $J = 4.0, 13.4$ Hz, CH₂), 3.04 (dd, 1H, $J = 4.0, 9.2$ Hz, CH), 3.92 (t, 2H, $J = 6.4$ Hz, CH₂), 6.92 (d, 2H, $J = 8.8$ Hz, H_{Ar}), 7.22–7.33 (m, 8H, H_{Ar}), 7.43–7.45 (m, 4H, H_{Ar}); ¹³C NMR (100 MHz, CD₃OD): δ 10.8 (CH₃), 23.6 (CH₂), 34.2 (CH₂), 55.0 (CH), 67.7 (Cq), 70.5 (CH₂), 114.9 (2 \times CH), 127.9 (2 \times CH), 129.1 (4 \times CH), 130.5 (4 \times CH), 132.0 (2 \times CH), 137.2 (Cq), 146.0 (Cq), 146.1 (Cq), 159.3 (Cq), 172.3 (CO); MS (ESI): m/z 444 [M + Na]⁺; Anal. Calcd for C₂₅H₂₇NO₃S: C 71.23, H 6.46, N 3.32, found: C 71.44, H 6.54, N 3.30.

4.2.2.4. S-[1-(4-Butylphenyl)-1,1-diphenylmethyl]-L-penicillamine (17k). Starting alcohol = 1-(4-butylphenyl)-1,1-diphenylmethanol (**15k**). Yield: 30%; mp 123–125 °C; [α]₅₈₉²⁵ = +171 ($c = 0.54$ in MeOH); ¹H NMR (300 MHz, CD₃OD + D₂O): δ 0.93 (t, 3H, $J = 7.3$ Hz, CH₃), 1.30 (s, 3H, CH₃), 1.32–1.40 (m, 2H, CH₂), 1.42 (s, 3H, CH₃), 1.54–1.64 (m, 2H, CH₂), 1.85 (s, 1H, CH), 2.59 (t, 2H, $J = 7.5$ Hz, CH₂), 7.14 (d, 2H, $J = 8.3$ Hz, H_{Ar}), 7.19–7.34 (m, 6H, H_{Ar}), 7.56 (d, 2H, $J = 8.5$ Hz, H_{Ar}), 7.67–7.70 (m, 4H, H_{Ar}); ¹³C NMR (100 MHz, CD₃OD): δ 14.3 (CH₃), 23.4 (CH₂), 25.9 (CH₃), 27.9 (CH₃), 34.7 (CH₂), 36.1 (CH₂), 53.5 (Cq), 61.9 (CH), 69.2 (Cq), 127.9 (2 \times CH), 129.0 (6 \times CH), 130.7 (2 \times CH), 130.8 (2 \times CH), 130.9 (2 \times CH), 142.9 (Cq), 143.2 (Cq), 146.0 (Cq), 146.1 (Cq), 170.6 (CO); MS (ESI): m/z 470 [M + Na]⁺; Anal. Calcd for C₂₈H₃₃NO₂S: C 75.13, H 7.43, N 3.13, found: C 75.45, H 7.53, N 3.32.

4.2.2.5. S-[1,1-Diphenyl-1-(4-propoxyphenyl)methyl]-L-penicillamine (17l). Starting alcohol = 1,1-diphenyl-1-(4-propoxyphenyl)methanol (**15j**). Yield: 34%; mp 133–135 °C; [α]₅₈₉²⁵ = +69 ($c = 0.15$ in MeOH); ¹H NMR (300 MHz, CD₃OD + D₂O): δ 1.03 (t, 3H, $J = 7.1$ Hz, CH₃), 1.31 (s, 3H, CH₃), 1.43 (s, 3H, CH₃), 1.74–1.81 (m, 2H, CH₂), 1.92 (s, 1H, CH), 3.93 (t, 2H, $J = 6.0$ Hz, CH₂), 6.87 (d, 2H, $J = 8.4$ Hz, H_{Ar}), 7.20–7.30 (m, 6H, H_{Ar}), 7.56 (d, 2H, $J = 8.4$ Hz, H_{Ar}), 7.64–7.72 (m, 4H, H_{Ar}); ¹³C NMR (100 MHz, CD₃OD): δ 10.8 (CH₃), 23.7 (CH₂), 25.9 (CH₃), 28.4 (CH₃), 53.2 (Cq), 62.0 (CH), 69.2 (Cq), 70.5 (CH₂), 114.6 (2 \times CH), 127.8 (2 \times CH), 128.7 (4 \times CH), 129.5 (4 \times CH), 131.6 (2 \times CH), 137.3 (Cq), 146.0 (2 \times Cq), 159.6 (Cq), 172.6 (CO); MS (ESI): m/z 472 [M + Na]⁺; Anal. Calcd for C₂₇H₃₁NO₃S: C 72.13, H 6.95, N 3.12, found: C 71.99, H 7.00, N 3.11.

4.3. Biological studies

4.3.1. NS5B inhibition assay

Recombinant NS5B carrying the N-terminal histidine-tag was purified from the plasmid pThNS5BC Δ 21 expressed in *Escherichia coli* DH5 α by Ni-NTA chromatography [33,34]. The compounds were dissolved in dimethylsulfoxide (DMSO) as a 10 mM stock solution and stored at –20 °C. Serial dilutions were made in DMSO immediately prior to the assay. The activity of the compounds against HCV NS5B was evaluated by the standard primer dependent elongation assay as previously described [33,34]. Briefly, preliminary screening was performed in the presence or absence of 100 μ M STL or the indicated derivative in a reaction buffer containing 20 mM Tris–HCl (pH 7.0), 100 mM NaCl, 100 mM Na-glutamate, 0.1 mM DTT, 0.01% BSA, 0.01% Tween-20, 5% glycerol, 20 U/mL of RNasin, 20 μ M UTP, 2 μ Ci [α -³²P]UTP, 0.25 μ M polyrA/U₁₂, 100 ng NS5BC Δ 21 and 1 mM MnCl₂. Following 60 min incubation at 30 °C, reactions were terminated by the addition of chilled 5% trichloroacetic acid (TCA) containing 0.5 mM sodium pyrophosphate. Reaction products were precipitated on GF-B filters and quantified on a liquid scintillation counter. NS5B activity in the presence of DMSO control was set at 100% and that in the presence of the STL derivatives was determined relative to this control. Compounds exhibiting greater than 50% inhibition at 100 μ M were evaluated for their IC₅₀ values from dose-response curves employing 8–12 concentrations of the compounds in duplicate in two independent experiments. Curves were fitted to data points

using nonlinear regression analysis and IC₅₀ values were interpolated from the dose-response curves using GraphPad Prism 3.03 software.

4.3.2. Cell culture

BHK-NS5B-FRLuc reporter cells were grown in Dulbecco's modified Eagle's medium (DMEM) with 10% heat-inactivated fetal bovine serum, 5% antibiotic-antimycotic, 5% nonessential amino acid, 1 mg/mL G418 and 10 μ g/mL blasticidin. Huh7/Rep-Feo1b replicon reporter cells were cultivated in DMEM containing 10% fetal calf serum, 5% antibiotic and 0.5 mg/mL G418. All cell lines were incubated at 37 °C in the presence of 5% CO₂ supplement.

4.3.3. BHK-NS5B-FRLuc reporter assay

The effect of the compounds on intracellular NS5B RdRp activity was screened employing the BHK-NS5B-FRLuc reporter system as previously described [36]. Briefly, BHK-NS5B-FRLuc reporter cells were plated at a confluence of 1×10^4 cells/well in 96 well plates and incubated with DMSO (1%) or the indicated compound (100 μ M) for 42 h. Reporter gene expression was measured with a Dual-Glo Luciferase Assay Kit (Promega, USA) in accordance with the manufacturer's instructions. Effect of the compounds on cell viability was estimated as the relative levels of firefly luciferase in compound treated cells versus DMSO controls. The inhibitory effect of the compounds on the intracellular NS5B RdRp activity was evaluated from the percent reduction in RLuc to FLuc luminescence signal in compound treated cells versus DMSO controls.

4.3.4. Huh7/Rep-Feo1b reporter system

The effect of the compounds on HCV RNA replication was screened employing the Huh7/Rep-Feo1b replicon reporter cells as previously described [42]. Briefly, 1×10^4 Huh7/Rep-Feo1b cells were plated in 96 well plates and treated with 100 μ M concentration of the indicated compound or DMSO for 42 h. The concentration of DMSO in cell culture was kept constant at 1.0%. Cell viability was measured by the colorimetric MTS assay employing the Cell-Titer 96AQ_{ueous} one solution assay reagent (Promega, USA). Inhibitory effect of the compounds on HCV RNA replication was measured as the relative levels of firefly luciferase signals in compound treated cells versus DMSO controls.

Acknowledgments

This work was supported by the National Institute of Health Research Grants DK066837 and CA153147 to N.K.-B. We would like to thank Prof. Garland R. Marshall (Washington University of St. Louis - MO) for critical reading of the manuscript.

References

- [1] A. Wasley, M.J. Alter, Epidemiology of hepatitis C: geographic differences and temporal trends, *Semin. Liver Dis.* 20 (2000) 1–16.
- [2] A. Grakoui, H.L. Hanson, C.M. Rice, Bad time for Bonzo? Experimental models of hepatitis C virus infection, replication, and pathogenesis, *Hepatology* 33 (2001) 489–495.
- [3] G.M. Lauer, B.D. Walker, Hepatitis C virus infection, *N. Engl. J. Med.* 345 (2001) 41–52.
- [4] I. Saito, T. Miyamura, A. Ohbayashi, H. Harada, T. Katayama, S. Kikuchi, Y. Watanabe, S. Koi, M. Onji, Y. Ohta, et al., Hepatitis C virus infection is associated with the development of hepatocellular carcinoma, *Proc. Natl. Acad. Sci. USA* 87 (1990) 6547–6549.
- [5] J. Ruiz, B. Sangro, J.I. Cuende, O. Belloqui, J.I. Riezu-Boj, J.I. Herrero, J. Prieto, Hepatitis B and C viral infections in patients with hepatocellular carcinoma, *Hepatology* 16 (1992) 637–641.
- [6] J.H. Hoofnagle, A.M. di Bisceglie, The treatment of chronic viral hepatitis, *N. Engl. J. Med.* 336 (1997) 347–356.
- [7] J.M. Pawlotsky, Pathophysiology of hepatitis C virus infection and related liver disease, *Trends Microbiol.* 12 (2004) 96–102.

- [8] J.J. Feld, T.J. Liang, HCV persistence: cure is still a four letter word, *Hepatology* 41 (2005) 23–25.
- [9] P. Ferenci, Pegylated interferon plus ribavirin for chronic hepatitis C: the role of combination therapy today, tomorrow and in the future, *Minerva Gastroenterol. Dietol.* 52 (2006) 157–174.
- [10] J.M. Pawlotsky, Virology of hepatitis B and C viruses and antiviral targets, *J. Hepatol.* 44 (2006) S10–S13.
- [11] C. Sheridan, New Merck and Vertex drugs raise standard of care in hepatitis C, *Nat. Biotechnol.* 29 (2011) 553–554.
- [12] C. Rice, Perspective: miles to go before we sleep, *Nature* 474 (2011) S8.
- [13] K. Garber, Hepatitis C: move over interferon, *Nat. Biotechnol.* 29 (2011) 963–966.
- [14] Q.L. Choo, G. Kuo, A.J. Weiner, L.R. Overby, D.W. Bradley, M. Houghton, Isolation of a cDNA clone derived from a blood-borne non-A, non-B viral hepatitis genome, *Science* 244 (1989) 359–362.
- [15] K. Tsukiyama-Kohara, N. Iizuka, M. Kohara, A. Nomoto, Internal ribosome entry site within hepatitis C virus RNA, *J. Virol.* 66 (1992) 1476–1483.
- [16] V. Brass, D. Moradpour, H.E. Blum, Molecular virology of hepatitis C virus (HCV): 2006 update, *Int. J. Med. Sci.* 3 (2006) 29–34.
- [17] S.E. Behrens, L. Tomei, R. De Francesco, Identification and properties of the RNA-dependent RNA polymerase of hepatitis C virus, *EMBO J.* 15 (1996) 12–22.
- [18] C.H. Hagedorn, E.H. van Beers, C. De Staercke, Hepatitis C virus RNA-dependent RNA polymerase (NS5B polymerase), *Curr. Top. Microbiol. Immunol.* 242 (2000) 225–260.
- [19] D. Moradpour, V. Brass, E. Bieck, P. Friebe, R. Gosert, H.E. Blum, R. Bartenschlager, F. Penin, V. Lohmann, Membrane association of the RNA-dependent RNA polymerase is essential for hepatitis C virus RNA replication, *J. Virol.* 78 (2004) 13278–13284.
- [20] R. De Francesco, C.M. Rice, New therapies on the horizon for hepatitis C: are we close? *Clin. Liver Dis.* 7 (2003) 211–242 (xi).
- [21] A.D. Kwong, L. McNair, I. Jacobson, S. George, Recent progress in the development of selected hepatitis C virus NS3,4A protease and NS5B polymerase inhibitors, *Curr. Opin. Pharmacol.* 8 (2008) 522–531.
- [22] S. Bressanelli, L. Tomei, A. Roussel, I. Incitti, R.L. Vitale, M. Mathieu, R. De Francesco, F.A. Rey, Crystal structure of the RNA-dependent RNA polymerase of hepatitis C virus, *Proc. Natl. Acad. Sci. USA* 96 (1999) 13034–13039.
- [23] C.A. Lesburg, M.B. Cable, E. Ferrari, Z. Hong, A.F. Mannarino, P.C. Weber, Crystal structure of the RNA-dependent RNA polymerase from hepatitis C virus reveals a fully encircled active site, *Nat. Struct. Biol.* 6 (1999) 937–943.
- [24] H. Ago, T. Adachi, A. Yoshida, M. Yamamoto, N. Habuka, K. Yatsunami, M. Miyano, Crystal structure of the RNA-dependent RNA polymerase of hepatitis C virus, *Structure* 7 (1999) 1417–1426.
- [25] S. Bressanelli, L. Tomei, F.A. Rey, R. De Francesco, Structural analysis of the hepatitis C virus RNA polymerase in complex with ribonucleotides, *J. Virol.* 76 (2002) 3482–3492.
- [26] I. Musmuca, A. Caroli, A. Mai, N. Kaushik-Basu, P. Arora, R. Ragno, Combining 3-D quantitative structure-activity relationship with ligand based and structure based alignment procedures for in silico screening of new hepatitis C virus NS5B polymerase inhibitors, *J. Chem. Inf. Model.* 50 (2010) 662–676.
- [27] J.E. Silverman, M. Ciustea, A.M. Shudofsky, F. Bender, R.H. Shoemaker, R.P. Ricciardi, Identification of polymerase and processivity inhibitors of vaccinia DNA synthesis using a stepwise screening approach, *Antivir. Res.* 80 (2008) 114–123.
- [28] K.Y. Zee-Cheng, C.C. Cheng, Experimental antileukemic agents. Preparation and structure-activity study of S-trityl-L-cysteine and related compounds, *J. Med. Chem.* 13 (1970) 414–418.
- [29] S. Debonis, D.A. Skoufias, R.L. Indorato, F. Liger, B. Marquet, C. Laggner, B. Joseph, F. Kozielski, Structure-activity relationship of S-trityl-L-cysteine analogues as inhibitors of the human mitotic kinesin Eg5, *J. Med. Chem.* 51 (2008) 1115–1125.
- [30] H.Y. Kaan, D.D. Hackney, F. Kozielski, The structure of the kinesin-1 motor-tail complex reveals the mechanism of autoinhibition, *Science* 333 883–885, New York, N.Y.
- [31] H.Y. Kaan, J. Weiss, D. Menger, V. Ulaganathan, K. Tkocz, C. Laggner, F. Popowycz, B. Joseph, F. Kozielski, Structure-activity relationship and multidrug resistance study of new S-trityl-L-cysteine derivatives as inhibitors of Eg5, *J. Med. Chem.* 54 (2011) 1576–1586.
- [32] E. Weber, K. Skobridis, A. Wierig, I. Goldberg, Triaryl/methanol host compounds. Synthesis, crystalline complex formation and X-ray crystal structures of three inclusions species, *J. Inclusion Phenom. Mol.* 28 (1997) 163–179.
- [33] N. Kaushik-Basu, A. Bopda-Waffo, T.T. Talele, A. Basu, Y. Chen, S.G. Kucukguzel, 4-Thiazolidinones: a novel class of hepatitis C virus NS5B polymerase inhibitors, *Front. Biosci.* 13 (2008) 3857–3868.
- [34] N. Kaushik-Basu, A. Bopda-Waffo, T.T. Talele, A. Basu, P.R. Costa, A.J. da Silva, S.G. Sarafianos, F. Noel, Identification and characterization of coumestans as novel HCV NS5B polymerase inhibitors, *Nucleic Acids Res.* 36 (2008) 1482–1496.
- [35] Y. Chen, A. Bopda-Waffo, A. Basu, R. Krishnan, E. Silberstein, D.R. Taylor, T.T. Talele, P. Arora, N. Kaushik-Basu, Characterization of aurintricarboxylic acid as a potent hepatitis C virus replicase inhibitor, *Antivir. Chem. Chemother.* 20 (2009) 19–36.
- [36] J.C. Lee, C.K. Tseng, K.J. Chen, K.J. Huang, C.K. Lin, Y.T. Lin, A cell-based reporter assay for inhibitor screening of hepatitis C virus RNA-dependent RNA polymerase, *Anal. Biochem.* 403 (2010) 52–62.
- [37] Y. Itsui, N. Sakamoto, S. Kakinuma, M. Nakagawa, Y. Sekine-Osajima, M. Tasaka-Fujita, Y. Nishimura-Sakurai, G. Suda, Y. Karakama, K. Mishima, M. Yamamoto, T. Watanabe, M. Ueyama, Y. Funaoka, S. Azuma, M. Watanabe, Antiviral effects of the interferon-induced protein guanylate binding protein 1 and its interaction with the hepatitis C virus NS5B protein, *Hepatol.* 50 (2009) 1727–1737 Baltimore, Md.
- [38] O. Trott, A.J. Olson, AutoDock Vina: improving the speed and accuracy of docking with a new scoring function, efficient optimization, and multi-threading, *J. Comput. Chem.* 31 (2010) 455–461.
- [39] A.C. Wallace, R.A. Laskowski, J.M. Thornton, LIGPLOT: a program to generate schematic diagrams of protein-ligand interactions, *Protein Eng.* 8 (1995) 127–134.
- [40] J. Barluenga, F.J. Fananas, R. Sanz, C. Marcos, M. Trabada, On the reactivity of o-lithioaryl ethers: tandem anion translocation and Wittig rearrangement, *Org. Lett.* 4 (2002) 1587–1590.
- [41] Y. Kawakami, Y. Sakai, A. Okada, Synthesis and polymerization of mono-p-alkoxy-substituted triphenylmethyl acrylate, *Polym. J.* 22 (1990) 705–718.
- [42] K. Kim, K.H. Kim, H.Y. Kim, H.K. Cho, N. Sakamoto, J. Cheong, Curcumin inhibits hepatitis C virus replication via suppressing the Akt-SREBP-1 pathway, *FEBS Lett.* 584 (2010) 707–712.

Cyclophilin A and Nuclear Factor of Activated T Cells Are Essential in Cyclosporine-Mediated Suppression of Polyomavirus BK Replication

Y. J. Li^{a,b}, H. H. Wu^{a,b}, C. H. Weng^{a,b},
Y. C. Chen^a, C. C. Hung^a, C. W. Yang^a,
R. Y. L. Wang^c, N. Sakamoto^d and Y. C. Tian^{a,*}

^aKidney Research Center, Department of Nephrology, Chang Gung Memorial Hospital, Taipei, Taiwan and Chang Gung University, Tao Yuan, Taiwan

^bGraduate Institute of Clinical Medical Sciences, Chang Gung University, Taiwan

^cDepartment of Biomedical Sciences, Chang Gung University, TaoYuan, Taiwan

^dDepartment of Gastroenterology and Hepatology, Tokyo Medical and Dental University, Tokyo, Japan

*Corresponding author: Ya-Chung Tian,
dryctian@adm.cgmh.org.tw

[Correction made after online publication May 29, 2012: author affiliations have been updated.]

Immunosuppressants have impacts on the development of polyomavirus-associated nephropathy. We previously demonstrated that cyclosporin A (CsA) suppressed polyomavirus BK (BKV) replication. The role of cyclophilin A (CypA) and nuclear factor of activated T cells (NFAT) in CsA-imposed suppression of BKV replication was determined in this study. Results demonstrated that knockdown of CypA but not CypB significantly reduced BKV large T antigen (TAg) expression and BKV titer. Overexpression of CypA reversed CypA siRNA-induced inhibition in BKV TAg expression. In addition, CypA overexpression attenuated the suppressive effect of CsA on TAg expression, suggesting CypA implicated in CsA-mediated anti-BKV effect. Knockdown of NFATc3 abrogated TAg expression, while overexpression of NFATc3 promoted TAg expression and augmented BKV promoter activity. NFATc3 binding to the BKV promoter was verified by chromatin immunoprecipitation assay and electrophoretic mobility shift assay. Renal histology also displayed an increase in NFATc3 expression in tubulointerstitium of BKV-associated nephropathy. Furthermore, overexpression of NFATc3 rescued CsA-mediated inhibition of BKV load and TAg expression. A CsA analog, NIM811, which cannot block NFAT functionality, failed to suppress TAg expression. In conclusion, CypA and NFAT are indispensable in BKV replication. CsA inhibits BKV replication through CypA and NFAT, which may be potential targets of anti-BKV treatment.

Key words: Cyclophilin, cyclosporine, nuclear factor of activated T cell, polyomavirus BK

Abbreviations: BKV, polyomavirus BK; PVAN, polyomavirus-associated nephropathy; CMV, cytomegalovirus; CsA, cyclosporin A; CypA, cyclophilin A; HCV, hepatitis C virus; HIV, human immunodeficiency virus; TAg, large T antigen; NCCR, noncoding control region; NFAT, nuclear factor of activated T cells.

Received 25 May 2011, revised 29 March 2012 and accepted for publication 10 April 2012

Introduction

Polyomavirus BK (BKV) reactivation in renal transplant patients is a critical problem (1,2). It has been reported that 5–10% of the subjects develop polyomavirus-associated nephropathy (PVAN) (3) and up to 50% of the patients with PVAN eventually lose their allograft within 2–3 years (4). Tacrolimus and mycophenolate are associated with a higher incidence of PVAN compared with other immunosuppressants (5, 6). Cyclosporin A (CsA), a calcineurin inhibitor, has been commonly used for the prevention of allograft rejection after organ transplantation due to its selective function in inhibiting T cell immunity. In addition to immunosuppression, CsA can also inhibit replication of various viruses, including human immunodeficiency virus (HIV) type 1, vaccinia virus, herpes simplex virus, hepatitis C virus (HCV) and cytomegalovirus (CMV) (7–12). It has been reported that CsA can inhibit BKV replication in green monkey kidney cells (Vero E6 cells) (13). Similarly, we previously demonstrated that CsA suppressed BKV replication and its noncoding control region (NCCR) promoter activity in cultured human renal proximal tubular cells (14). Nevertheless, the mechanisms by which CsA inhibits BKV replication remain elusive.

Cyclophilin A (CypA) was isolated as a CsA-specific binding protein by Handschumacher et al. in 1984 (15). To date, seven major cyclophilin (Cyp) members including CypA, CypB, CypC, CypD, CypE, Cyp40 and CypNK have been identified in humans (16). CsA binds to cyclophilins to form a complex and subsequently inhibits phosphatase activity that is required for calcineurin activation. Through inhibition of calcineurin activation, CsA induces phosphorylation of nuclear factor of activated T cells (NFAT), which prevents translocation of NFAT from the cytoplasm into the nucleus, thereby blocking NFAT activity (17,18). Five NFAT

family members have been identified to date. Of these, NFATc1 (NFAT2), NFATc2 (NFAT1), NFATc3 (NFAT4) and NFATc4 (NFAT3) are dephosphorylated and activated by calcineurin, while they are phosphorylated and inactivated by CsA (19,20).

Cyp and NFAT, two CsA mediators, have been shown to play important roles in CsA-induced suppression of different viral replication. For example, CsA inhibits mouse CMV and HCV replications via a CypA-dependent pathway (11,21). In addition, NFAT can enhance HIV-1 replication in primary human CD4 T cells (22). In this study, we demonstrated that CypA and NFATc3 are essential for CsA-mediated suppression of BKV replication. This study may provide a new therapeutic target for the treatment of BKV infection.

Materials and Methods

Materials and cell culture

Mouse anti-SV40 TAg antibody, which can also recognize BKV TAg, was purchased from Calbiochem (La Jolla, CA, USA). Anti-BKV VP1 antibody was the gift of Abnova Co. (Taipei, Taiwan). Antiflag antibody and CsA were purchased from Sigma (Sigma Chemical Company Ltd., Poole, UK). CypA, CypB and NFATc3 siRNA were obtained from Dharmacon Inc. (Lafayette, CO, USA). Goat anti-NFATc3 antibody was purchased from R&D Systems (Minneapolis, MN, USA) and rabbit anti-NFATc4 antibodies were purchased from Santa Cruz Biotech, Inc. (Santa Cruz, CA, USA).

Immortalized human renal proximal tubular cells, HK-2, were cultured as described previously (23).

Flag-epitope (DYKDDDDK) cDNA was attached to the full-length coding sequences of CypA, CypB, NFATc3 and NFATc4, which are obtained by qPCR from human genomic DNA using the standard technique (24).

Real-time quantitative polymerase chain reaction (qPCR)

qPCR was performed as described previously (25). Briefly, total RNA was isolated from cells and reverse-transcribed to DNA. qPCR was performed according to the manufacturer's instructions using an ABI-Prism 7700 with SYBR Green I (PE-Applied Biosystems, Cheshire, UK, Britain). Primers used to assay BKV TAg and glyceraldehyde-3-phosphate dehydrogenase (GAPDH) transcript levels (BKV TAg: 5-CTGTCCCTAAAACCTGCAA-3 and 5-GCCTTTCCTTCCATCAACA-3; GAPDH: 5-TTCCAGGAGCGAGATCCCT-3 and 3-CACCCATGACGAACATGGG-5) were constructed to be compatible with a single reverse transcription-PCR thermal profile (95°C for 10 min, 40 cycles of 95°C for 30 s and 60°C for 1 min). Experimental results are presented as the transcript level of the analyzed genes relative to GAPDH transcript level.

To determine viral load, BKV and cellular DNA were extracted from cell lysate using a QIAamp[®] DNA Mini Kit (Qiagen, Hilden, Germany). qPCR was performed as described above. The BKV DNA was normalized by analyzing samples in parallel by the quantitative PCR for the cellular tubulin β 2A DNA using the commercial primers and probes (Hs00742533_s1*, probe: GTCTCAAGCATGGTCTTCTACTT; Applied Biosystems).

Gene silencing by short interfering RNA (siRNA)

RNA interference was used to reduce CypA, CypB and NFATc3 expressions. Briefly, 0.5–1.5 μ g of siRNA against CypA, CypB, NFATc3 or control siRNA

was diluted in the serum-free medium to give a final volume of 100 μ L. Subsequently, RNAiFectl transfection reagent was mixed with diluted siRNA at ratio from 6:1 to 3:1. Following incubation for 15 min at room temperature, the mixture was added to the culture medium.

Luciferase assay

The NCCR of the BKV and BKV TAg were constructed as described previously (14). The BKV NCCR in early and late orientation was used in this study. Luciferase assays utilized the Dual-Luciferase Report Assay (Promega, Madison, WI, USA) applied according to the manufacturer's recommendations. Luciferase activity was measured using a luminometer (MLX micro titer plate luminometer, Dynex Ltd., Chantilly, VA, USA) and examined on duplicates of each sample. Experimental results were presented as firefly luciferase activity normalized to Renilla luciferase activity.

Western blot analysis

Total cellular protein extraction was performed as described previously (26). Protein samples mixed with reducing SDS sample buffer were resolved on a 10% SDS-PAGE and then electroblotted. Nonspecific binding was blocked with a 5% nonfat milk solution. The membrane was then incubated with primary antibody overnight at 4°C followed by incubation with a horseradish peroxidase (HRP) conjugated secondary antibody. Proteins were visualized using enhanced chemiluminescence (Amersham Biosciences, Amersham, UK). Protein bands of Western blot analysis were quantified using Quantity One software (BioRad). The density of each protein band was normalized with that of tubulin.

Chromatin immunoprecipitation

DNA was cross-linked with 1% formaldehyde at 37°C for 10 min and cells were then resuspended in a SDS lysis buffer. Cell lysate was sonicated and supernatants were diluted 10-fold in a ChIP dilution buffer and precleared with salmon sperm DNA/protein A agarose 50% slurry (Millipore, Billerica, MA, USA). Following brief centrifugation, the supernatant fraction was immunoprecipitated with rabbit anti-NFATc3 or anti-NFATc4 overnight. After the addition of protein A agarose slurry, samples were incubated for 1 h at 4°C. Pellet agarose was washed once with wash buffer I (Millipore, Billerica, USA) and buffer II (Millipore, Billerica, MA, USA). DNA was eluted in 1% SDS, 0.1 M NaHCO₃ at room temperature for 1 h. Following proteinase K digestion, DNA was recovered with phenol/chloroform extraction and ethanol precipitation. After the addition of glycogen, DNA was amplified by qPCR using SYBR Green Master Mix as described above. Primers were designed for the BKV NCCR as follows: forward 5'-GCAAAAATTGCAAAAGAATAGG-3' and reverse 5'-TTCCAGTCCAGGTTTACCAA-3'.

Electrophoretic mobility shift assay

Electrophoretic mobility shift assay (EMSA) was employed for the analysis of NCCR DNA binding ability by the purified recombinant NFATc3 and NFATc4 protein. Briefly, the pGEX vector for expression in BL21 (DE3) *Escherichia coli* (Merck) was used to produce the GST-tagged recombinant proteins. Proteins were over-expressed through induction with 0.2 mM Isopropyl β -D-1-thiogalactopyranoside (IPTG) at 16°C for 10 h. Both of the recombinant NFATc3 and NFATc4 were purified through affinity chromatography. For NFAT-DNA binding followed by EMSA, essentially a 20 μ L reaction comprised of purified protein, ³²p-labelled double-stranded DNA (BKV NCCR) and 125 μ g/ μ L poly dl-dC buffered in 12 mM HEPES pH 7.8, 75 mM KCl, 1 mM EDTA, 4 mM GTP and 12.5% glycerol was incubated at room temperature for 1 h. The protein-DNA mixtures were subsequently loaded onto a 6% DNA Retardation Gel (Invitrogen) alongside "no protein" and "no DNA" controls, and migrated in a 0.5 \times TBE running buffer for 1.5 h. Competition experiments were performed with 100-fold excess of the respective unlabelled probes.

Viral progeny

Viral progeny is measured as described by Moriyama et al. (27). Briefly, infected cells were extracted and lysates were undiluted or diluted to 1:10 or 1:100 and then seeded on cells in 8-well chamber slides for 72 h. Cells were then fixed with 3% paraformaldehyde and permeabilized with 0.2% Triton in PBS. Subsequently, cells were incubated with the mouse anti-SV40 TAG antibody overnight and then incubated with FITC-conjugated antibody for 1 h. Slides were finally mounted using the Vectashield mounting medium (Vector Laboratories) containing 4',6'-diamidino-2-phenylindole (dapi) (Molecular Probes, California, USA) to stain nuclei. The fluorescence-forming unit was calculated according to the protocol (27).

Immunohistochemistry

Under permission of the ethics committee of our hospital, residual renal biopsy specimens obtained from 2 PVAN patients were analyzed for deposition of NFATc3 and TAG expressions. Normal tissue away from the edge of renal cell carcinoma (RCC) obtained from one RCC patient undergoing nephrectomy was used as a negative control. Kidney specimens were fixed with 4% paraformaldehyde and embedded in paraffin. Following deparaffinization, sections were then immersed in 3% H₂O₂ in methanol and blocked with 5% bovine albumin/PBS for 20 min. Following incubation with anti-NFATc3 or anti-SV40 TAG for 1 h, sections were treated with relevant biotin-conjugated antibodies and the NFATc3 or TAG immunostaining was then displayed using a Vectastain ABC kit (Vector Laboratories).

Statistical analysis

All the data were presented as means ± SEM. Statistical analysis was performed using the unpaired Student's *t*-test. A value of *p* < 0.05 was considered to represent a significant difference.

Results

Inhibition of CypA but not CypB expression reduced BKV replication

To determine whether CypA is required in BKV (TU strain) replication, endogenous CypA expression was knocked down by gene silencing. Inhibition of CypA expression by CypA siRNA was confirmed by Western blot analysis which showed a significant decrease in CypA protein expression (Figure 1A). Blockade of CypA expression led to a reduction in BKV TAG expression (Figure 1A). Similarly, inhibition of CypA expression resulted in a decrease in the level of TAG transcripts as determined by qPCR (Figure 1B).

To assess whether CypA knockdown-mediated inhibition of BKV replication could be rescued by reintroduction of CypA into cells, endogenous CypA expression was suppressed using CypA siRNA followed by CypA overexpression. Following inhibition of CypA expression, BKV TAG expression was suppressed while BKV TAG expression was enhanced after the reintroduction of CypA into cells (Figure 2A). Similarly, the results of qPCR also confirmed that the reintroduction of CypA into cells led to an increase in the level of TAG transcripts (Figure 2B) and viral load (Figure 2C). To measure the infectious progeny, viral lysates were collected at the end of the experiments and seeded on the new cells for 72 h. The result confirmed that knockdown of

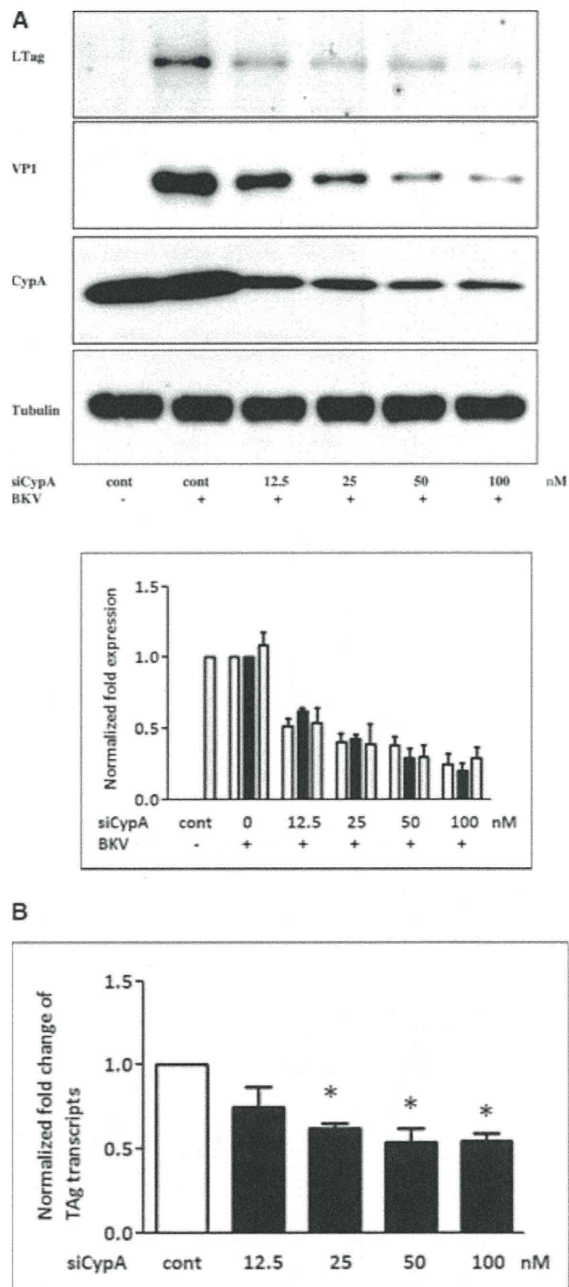


Figure 1: Inhibition of CypA reduced BKV TAG expression. HK-2 cells were transfected with siCypA at different concentrations (12.5–100 nM) overnight. Cells were then infected with the BKV (1.0 × 10⁶ copies/mL) for further 72 h under serum-free condition. Cells transfected with scramble siRNA as the control (100 nM). Cell lysate was subjected to Western blot analysis to determine BKV TAG expression (A) or qPCR to assess the levels of BKV TAG transcripts (B). The density of each protein band (TAG: white bar, VP1: black bar, CypA: gray bar) was normalized with that of tubulin and the fold changes compared to the control were displayed in the lower panel. One representative result of Western blot analysis from three individual replicate experiments is shown. Results of qPCR are expressed as the relative fold increase of TAG transcripts over that of the control, which is arbitrarily set to one (**p* < 0.05).

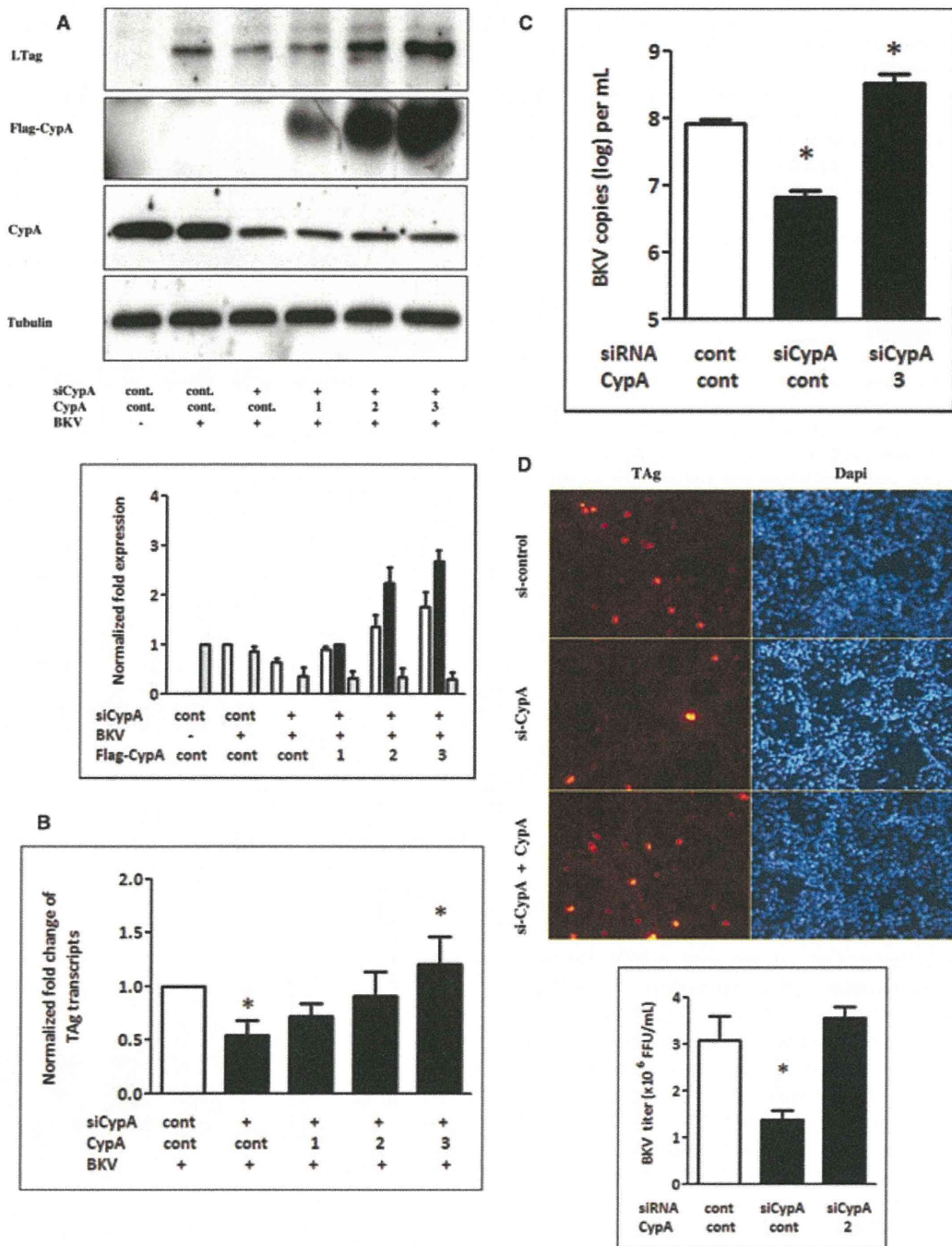


Figure 2: CypA knockdown-induced suppression of BKV TAG expression was rescued by reintroduction of CypA. Cells were transfected with CypA siRNA (50 nM) or scramble siRNA (control) overnight and washed with medium followed by transfection with different concentrations (1–3 µg/mL) of plasmids expressing flag-tagged CypA or an empty control vector. Cells were then infected with the BKV (1.0×10^6 copies/mL) for further 72 h. Cell lysate was subjected to Western blot analysis to determine BKV TAG expression (A) or qPCR to assess the levels of BKV TAG transcripts (B) and viral load. (C) The density of each protein band (TAG: white bar, Flag-tagged CypA: black bar, endogenous CypA: gray bar) was normalized with that of tubulin and the fold changes compared to the control were displayed in the lower panel. For unknown reasons, the flag-tagged CypA expression was unable to be detected by anti-CypA antibody. Results of qPCR are expressed as the relative fold increase of TAG transcripts over that of the control, which is arbitrarily set to one. (* $p < 0.05$ vs. control). (D) At the end of the experiments performed under the above condition, viral lysates were collected and seeded on the new cells for 72 h. Intracellular viral load was then determined by counting the TAg immunostaining-positive cells (upper panel) to calculate fluorescence-forming units (FFU) as described in the Materials and Methods section.

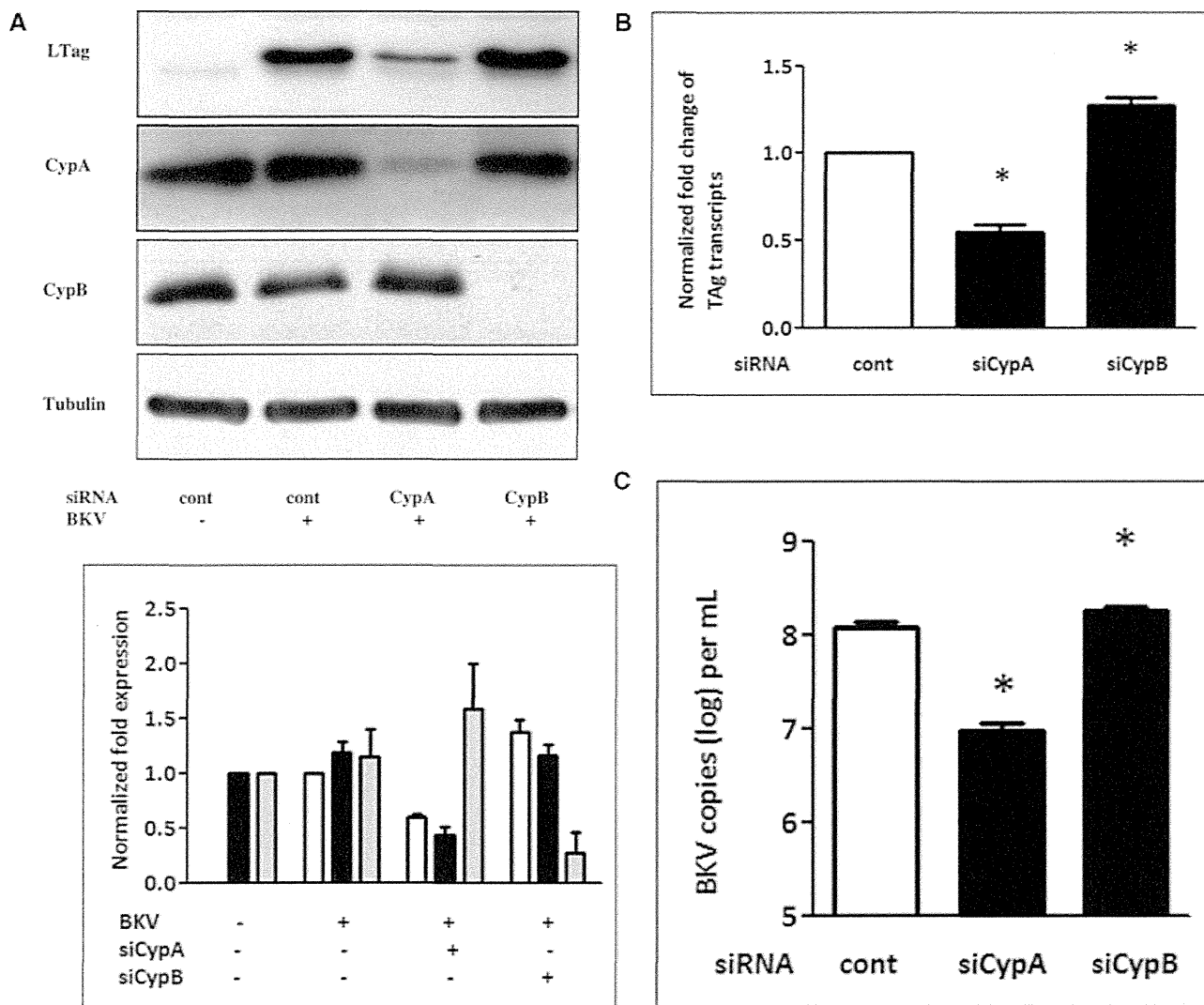


Figure 3: Inhibition of CypA but not CypB reduced BKV TAG expression. Cells were transfected with siCypA or siCypB (50 nM) overnight. Cells were then infected with the BKV (1.0×10^6 copies/mL) for further 72 h under serum-free condition. Cells transfected with scramble siRNA as the control. Cell lysate was subjected to Western blot analysis to determine BKV TAG expression (A) or qPCR to assess the levels of BKV TAG transcripts (B) and viral load (C). The density of each protein band (TAG: white bar, CypA: black bar, CypB: gray bar) was normalized with that of tubulin and the fold changes compared to the control were displayed in the lower panel. Results of qPCR are expressed as the relative fold increase of TAG transcripts over that of the control, which is arbitrarily set to one (* $p < 0.05$).

CypA reduced BKV load and the reintroduction of exogenous CypA restored this inhibition (Figure 2D).

In addition to CypA, it has been reported that CypB is also required for viral replication (28, 29). To establish whether CypB participates in BKV replication, endogenous CypB expression was inhibited by CypB siRNA. Western blot analysis showed that, in contrast to CypA, knockdown of CypB slightly increased BKV TAG expression (Figure 3A). Similarly, inhibition of CypB expression slightly enhanced the level of TAG transcripts (Figure 3B) and viral load (Figure 3C). These results suggest an indispensable role of CypA but not CypB in BKV replication.

CypA overexpression attenuated CsA-mediated suppression of BKV replication

To assess whether CypA is crucial in CsA-mediated inhibition of BKV replication, cells were transfected with the CypA-expressing plasmids followed by administration of CsA for 72 h. In accordance with our previous study (14), administration of CsA (1 μ g/mL) resulted in a reduction in BKV TAG expression. Importantly, overexpression of CypA significantly attenuated CsA-mediated inhibition in BKV TAG expression compared with transfection of the control vector (Figure 4). At high CypA expression levels, CypA overexpression even surpassed the CsA-mediated inhibitory effect

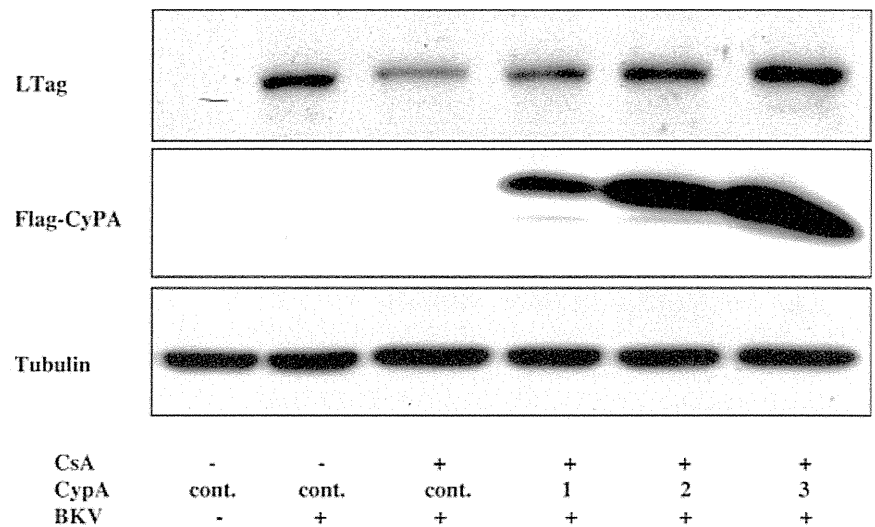
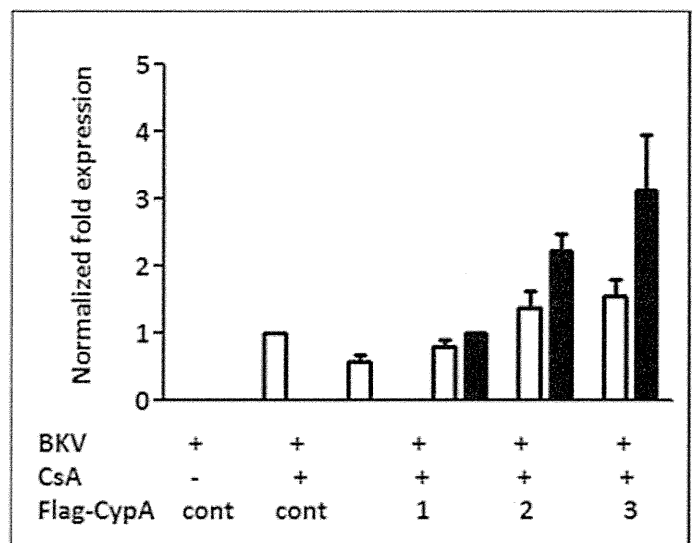


Figure 4: The suppressive effect of CsA on BKV TAG expression was attenuated by overexpression of CypA.

Cells were transfected with different concentrations (1–3 $\mu\text{g}/\text{mL}$) of plasmids expressing flag-tagged CypA or an empty control vector. Cells were then infected with the BKV (1.0×10^6 copies/mL) in the presence or absence of CsA (1 $\mu\text{g}/\text{mL}$) under serum-free condition for 72 h. Cell lysate was subjected to Western blot analysis to determine BKV TAG expression (A) or BKV DNA copies (B). The density of each protein band (TAG: white bar, flag-tagged CypA: black bar) was normalized with that of tubulin and the fold changes compared to the control were displayed in the lower panel. One experiment representative of three individual replicate experiments is shown.



and led to a significant enhancement in BKV TAG expression.

NFAT is crucial for BKV replication

Since NFAT is a major downstream transcription factor of the cyclophilin/calcineurin complex (30), we therefore assessed whether NFAT plays a role in BKV replication. Results demonstrated that NFATc3 and NFATc4 were prominently expressed in HK-2 cells, whereas NFATc1 and NFATc2 were weakly detected in cells (data not shown). To clarify the effect of NFATc3 and NFATc4 on BKV replication, NFATc3 or NFATc4 was overexpressed overnight, followed by addition of BKV to cells. The result demonstrated that overexpression of NFATc3 enhanced BKV TAG expression (Figure 5A). Similarly, NFATc4 overexpression

also facilitated BKV TAG expression (Figure 5B). These results indicate that there is a stimulatory effect of NFATc3 and NFATc4 on BKV replication.

BKV NCCR is the main regulatory region of BKV replication. To assess whether NFAT can regulate BKV NCCR, plasmids expressing NFATc3 or NFATc4 and the BKV NCCR luciferase reporter in early or late orientation were co-transfected in cells. NFATc3 or NFATc4 overexpression led to an increase in promoter activity of the BKV NCCR luciferase reporter in early orientation, reaching a 2.9- or 3.4-fold increase respectively when compared with that of the mock transfection (Figure 5C). Similarly, the activity of the late NCCR promoter reporter was increased 2.5- or 2.7-fold, respectively, by NFATc3 or NFATc4 overexpression (Figure 5D).

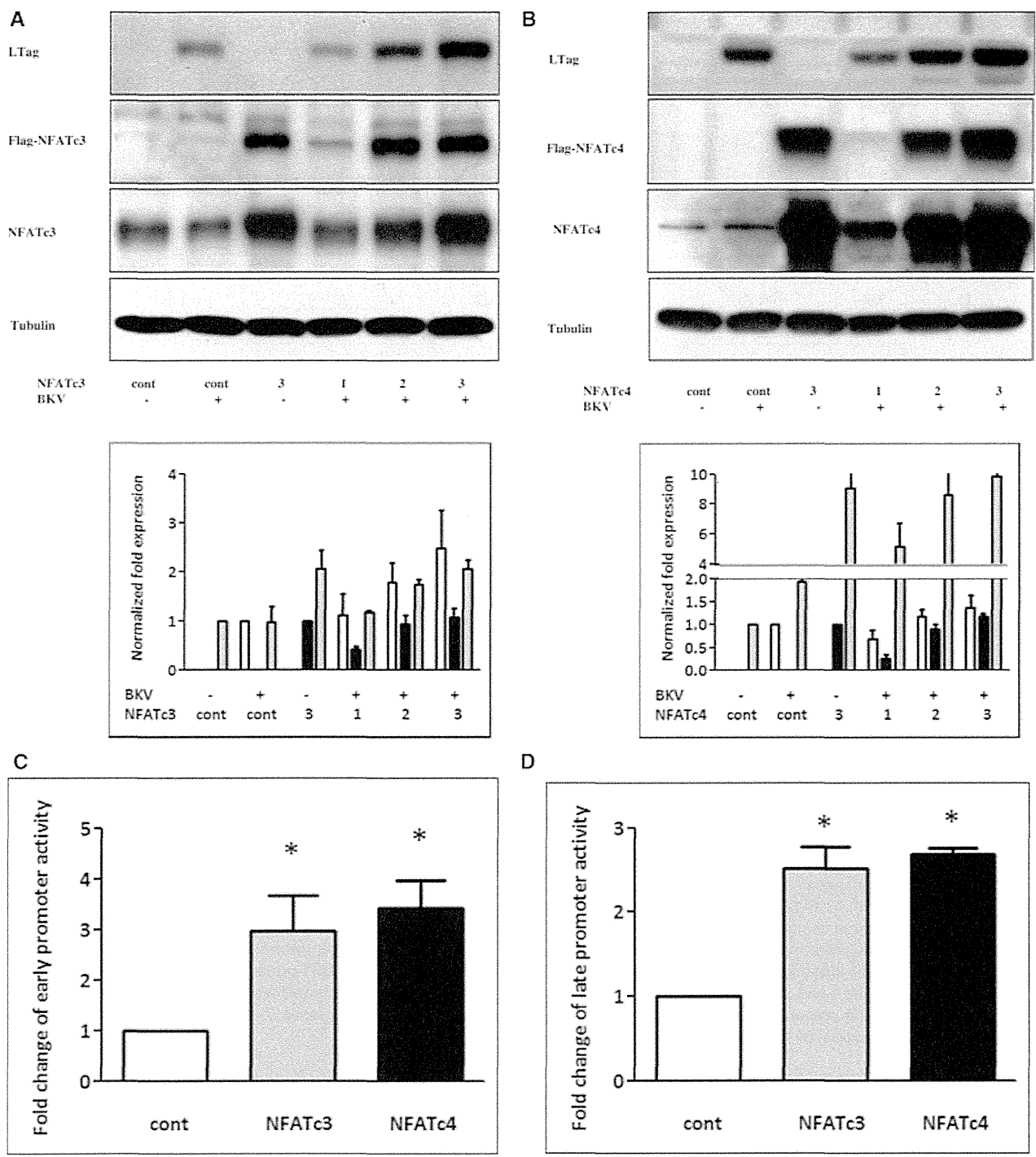


Figure 5: NFAT overexpression enhanced BKV TAG and the BKV NCCR activity. (A and B) Cells were transfected with plasmids expressing NFATc3 (A) or NFATc4 (B) overnight and then infected with the BKV (1.0×10^6 copies/mL) for further 72 h. Cell lysate was subjected to Western blot analysis to determine BKV TAG expression. The density of each protein band (TAG: white bar, flag-tagged NFATc3 or NFATc4: black bar; total NFATc3 or NFATc4: gray bar) was normalized with that of tubulin and the fold changes compared to the control were displayed in the lower panel. (C and D) The NCCR firefly luciferase reporter vector (1 μ g/mL) in early (C) or late orientation (D), the *Renilla* luciferase vector (1 μ g/mL), the plasmids expressing NFATc3 (3 μ g/mL) (gray bar) or NFATc4 (3 μ g/mL) (black bar) or the control vector (white bar) were cotransfected into HK-2 cells overnight. Cells were grown under serum-free condition for further 48 h. Luciferase assays were then performed on duplicate samples and the firefly luciferase activity was normalized to that of *Renilla* luciferase activity. The results were obtained from four independent experiments (* $p < 0.05$).

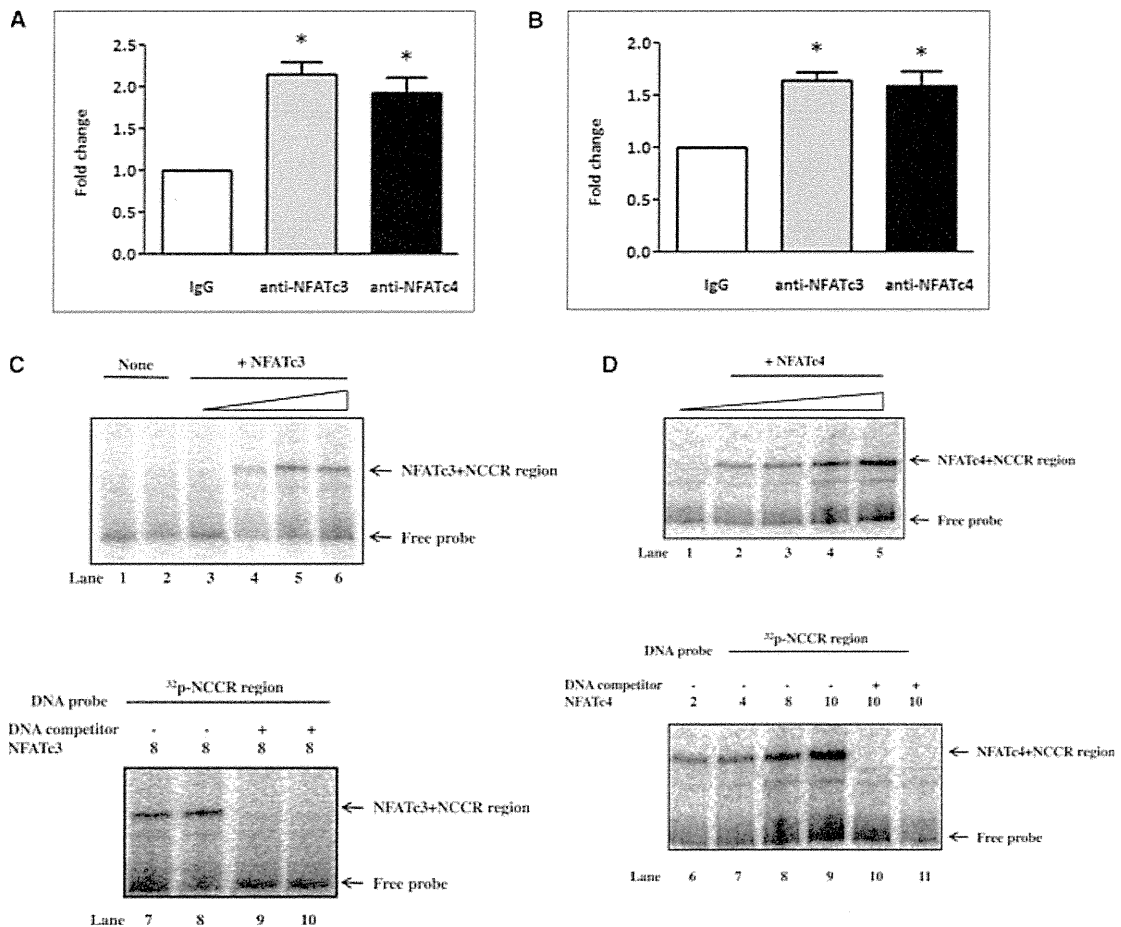


Figure 6: NFAT binds to the BKV promoter. (A and B) Cells were transfected with the plasmids expressing the BKV NCCR (A) or infected with BKV (1.0×10^6 copies/mL) (B) for 48 h. Cells were then subjected to the ChIP assay described in the Materials and Methods section. Immunoprecipitated DNA by anti-NFATc3 (gray bar), anti-NFATc4 (black bar) or a nonspecific IgG antibody (white bar) was quantified by qPCR using primers detecting the BKV NCCR. Results are expressed as the relative fold increase of the NFATc3 or NFATc4-associated DNA over that of the nonspecific IgG control, which is arbitrarily set to one. All data are represented as mean \pm SE from four independent experiments (* $p < 0.05$). (C and D) Interaction of NFATc3, NFATc4 with BKV noncoding control region was assessed by EMSA. Binding complexes were separated using 6% nondenaturing PAGE as described in the Materials and Methods section. Labeled double-stranded oligonucleotides, NCCR, were mixed with purified recombinant NFATc3 (C) in the final concentration of 0, 2, 4, 8 $\mu\text{g}/\mu\text{L}$ (lanes 3 and 6) and recombinant NFATc4 in the final concentration of 0, 2, 4, 8, 10 $\mu\text{g}/\mu\text{L}$ (D: lanes 1 and 5). GST protein was used for a negative control shown as 'none' (C: lanes 1 and 2). In the parallel experiments, NCCR oligonucleotides were mixed with 8 $\mu\text{g}/\mu\text{L}$ of purified recombinant NFATc3 or NFATc4 in the presence (C: lanes 9 and 10; D: lanes 10 and 11) or absence (C: lanes 7 and 8; D: lanes 6 and 9) of 100 \times unlabeled NCCR oligonucleotides as competitors.

To assess whether NFAT can bind to the BKV promoter, cells were transfected with the plasmids expressing BKV NCCR (Figure 6A) or infected with BKV (Figure 6B) for 48 h and chromatin was then immunoprecipitated with anti-NFATc3 or anti-NFATc4 antibody followed by qPCR to quantify the binding of the viral promoter to NFATc3 or NFATc4. Results of the ChIP assay demonstrated that the levels of the BKV promoter DNA binding to NFATc3 and NFATc4 were increased 2.1- and 1.9-fold, respectively, by transfection with the plasmids expressing BKV NCCR or increased 1.6- and 1.5-fold respectively by BKV infection when compared to that of the DNA immunoprecipitated with a nonspecific IgG antibody (Figures 6A and B). To sup-

port the results of the ChIP assay, we performed EMSA by *in vitro* mixture of recombinant NFATc3 or NFATc4 proteins and ^{32}p -labelled double-stranded DNA (BKV NCCR) prior to gel shift analysis. Results clearly demonstrated an increase in binding of NFATc3- (Figure 6C) and NFATc4 (Figure 6D) with BKV NCCR.

To further verify the role of NFAT in BKV replication, NFATc3 expression was suppressed by NFATc3 siRNA and cells were then infected with BKV. Western blot analysis showed that knockdown of NFATc3 expression reduced BKV TAG expressions (Figure 7A). Similarly, knockdown of NFATc3 by siRNA also reduced the promoter activity of

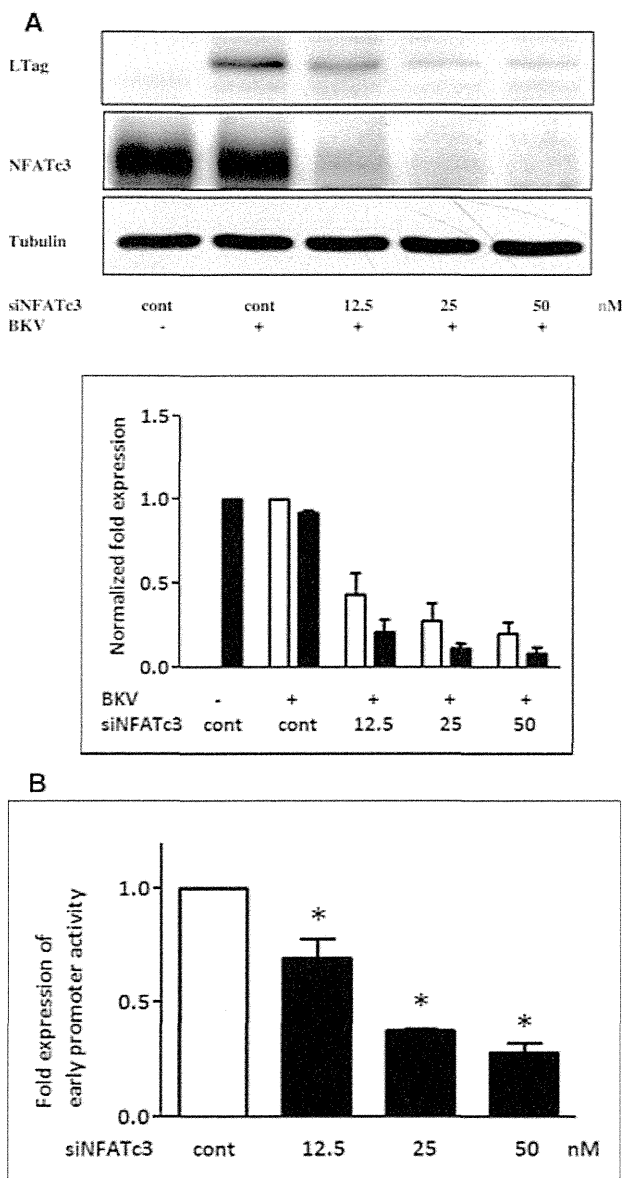


Figure 7: Inhibition of NFATc3 reduced BKV TAG expression. (A) Cells were transfected with NFATc3 siRNA at different concentrations (12.5–50 nM) overnight. Cells were then infected with the BKV (1.0×10^6 copies/mL) for further 72 h under serum-free condition. Cells were transfected with scramble siRNA as the control (50 nM). Cell lysate was subjected to Western blot analysis to determine BKV TAG expression. The density of each protein band (TAG; white bar, NFATc3; black bar) was normalized with that of tubulin and the fold changes compared to the control were displayed in the lower panel. One representative result of Western blot analysis from three individual replicate experiments is shown. (B) Cells were transfected with NFATc3 siRNA at different concentrations (12.5–50 nM) or scramble siRNA overnight. The NCCR firefly luciferase reporter plasmid and the *Renilla* luciferase plasmid were cotransfected into HK-2 cells for further 48 h. The firefly luciferase activity was normalized to that of *Renilla* luciferase activity. The results were obtained from three independent experiments (* $p < 0.05$ vs. the control).

2356

the BKV NCCR luciferase reporter (Figure 7B). These data confirm that NFAT are essential for BKV replication.

CsA-mediated inhibition of BKV replication was rescued by NFAT overexpression

CsA inhibits calcineurin activity and causes NFAT phosphorylation that inactivates NFATs and prevents subsequent nuclear translocation to trigger transcription of target genes in immune cells (31). To appreciate whether CsA can cause NFATc3 phosphorylation and then inactivate NFATc3 in HK-2 cells, CsA was added to HK-2 cells for 24 h. NIM811, a CsA derivative, which cannot inhibit calcineurin activity and cause NFAT activation, was used as a control. The results revealed that the administration of CsA led to slow migration of NFATc3, indicating phosphorylation and inactivation of NFATc3 activity by CsA (Figure 8A). In contrast, the addition of NIM811 did not result in slow migration of NFATc3, implying the lack of an inhibitory effect on NFATc3 activity. Interestingly, while CsA suppressed BKV TAG expression, NIM811 did not alter BKV TAG expression (Figure 8A). This result suggests that NFATc3 activity is implicated in CsA-mediated suppression of BKV replication.

To verify the crucial role of NFATc3 in CsA-imposed suppression of BKV replication, NFATc3 was overexpressed in the presence of CsA. Western blot analysis showed that NFATc3 or NFATc4 overexpression diminished the inhibitory effect of CsA on BKV TAG expressions, while overexpression of the control vector did not reverse CsA-mediated inhibition of BKV TAG expression (Figures 8B and C) and viral load (Figure 8D). In addition, NFATc3 or NFATc4 overexpression even surpassed the CsA-induced reduction in the BKV early promoter activity (Figure 8E). These results suggest that NFAT is essential mediators in CsA-mediated suppression of BKV replication.

NFAT expression is increased in PVAN

Since NFAT is crucial for BKV replication, NFATc3/NFATc4 expression in renal biopsy specimen obtained from two patients with PVAN was assessed. Results of immunohistochemistry revealed that NFATc3/NFATc4 staining was prominently increased in the cytoplasm and nuclei of renal tubules and interstitial lymphocytes in the kidney of PVAN (Figures 9B and F; NFATc4 staining: not shown) when compared with that of the normal control (Figures 9A and E). PVAN was confirmed as BKV TAG expression was detected in the tubules (Figures 9D and G).

Discussion

In this study, we demonstrate the importance of cyclophilin in regulation of both BKV early and late replication in HK-2 cells as knockdown of CypA-inhibited BKV LTag and VP1 expression. While CypA knockdown substantially suppressed BKV LTag and VP1 expressions, knockdown of CypB did not prominently affect BKV LTag and VP1 expression. Cyclophilins have been identified to play a crucial role in HIV

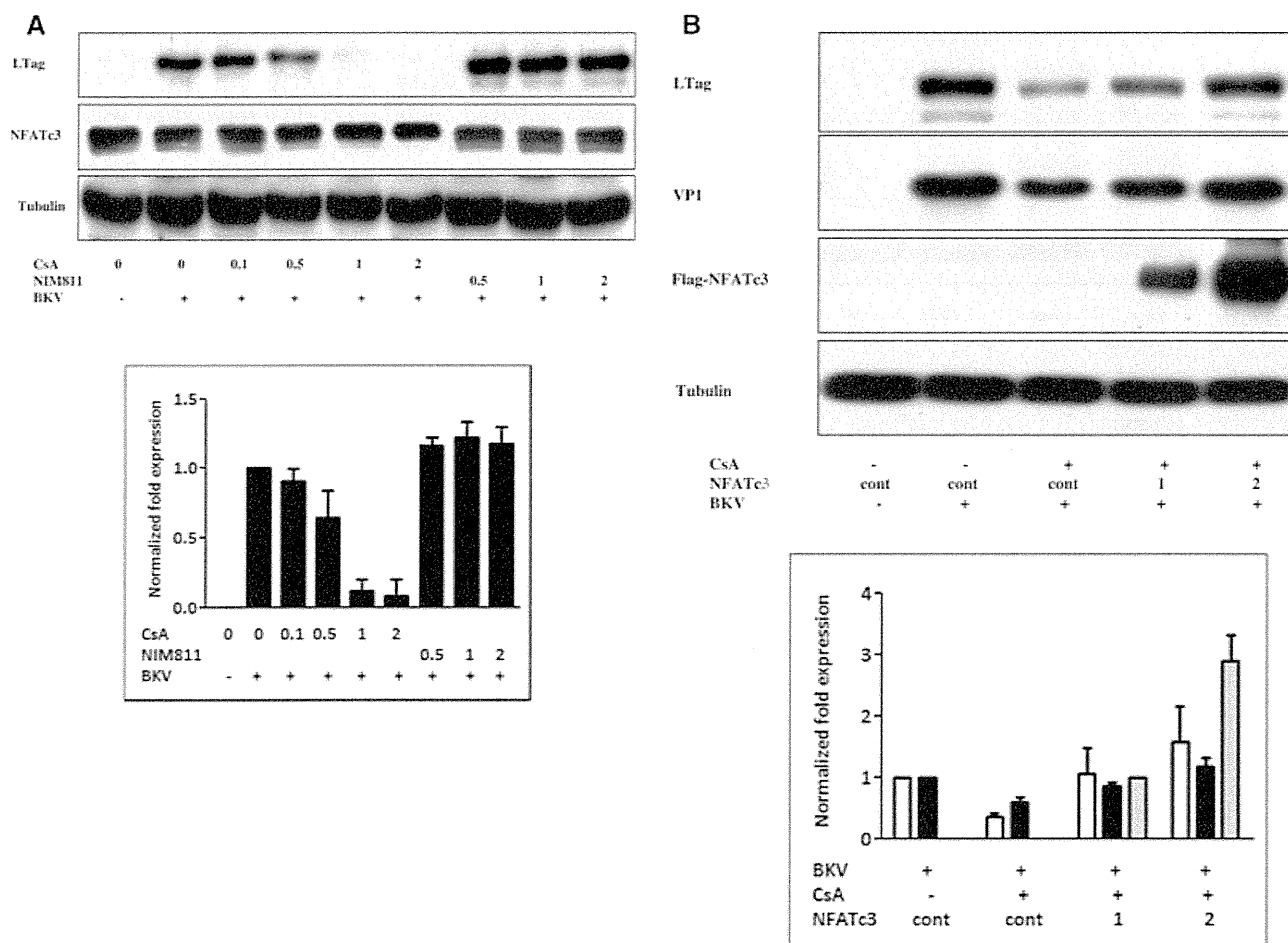


Figure 8: The suppressive effect of CsA on BKV TAG expression was attenuated by overexpression of NFATs. (A) Cells were infected with the BKV (1.0×10^6 copies/mL) in the presence or absence of CsA (0.5–2 $\mu\text{g}/\text{mL}$) or NIM811 (0.5–2 $\mu\text{g}/\text{mL}$) for 72 h. Cell lysate was subjected to Western blot analysis to determine NFATc3 and BKV TAG expression. (B and C) Cells were transfected with different concentrations (1–2 $\mu\text{g}/\text{mL}$) of plasmids expressing flag-tagged NFATc3 (B) or NFATc4 (C) or an empty control vector overnight. Cells were then infected with the BKV (1.0×10^6 copies/mL) in the presence or absence of CsA (1 $\mu\text{g}/\text{mL}$) under serum-free condition for 72 h. Cell lysate was subjected to Western blot analysis to determine BKV TAG expression or to qPCR for viral load (D). The density of each protein band (TAG: white bar, VP1: black bar, Flag-NFATc3/c4: gray bar) was normalized with that of tubulin and the fold-changes compared to the control were displayed in the lower panel. One experiment representative of three individual replicate experiments is shown. (E) The NCCR early promoter firefly luciferase reporter (1 $\mu\text{g}/\text{mL}$), the *Renilla* luciferase vector (1 $\mu\text{g}/\text{mL}$), the plasmids expressing NFATc3 (3 $\mu\text{g}/\text{mL}$) (gray bar) or NFATc4 (3 $\mu\text{g}/\text{mL}$) (black bar) or the control vector (white bar) were cotransfected into HK-2 cells overnight. Cells were incubated in the presence or absence of CsA (1 $\mu\text{g}/\text{mL}$) for further 48 h. The firefly luciferase activity was normalized to that of *Renilla* luciferase activity. The results were obtained from four independent experiments. (* $p < 0.05$ vs. the control, # $p < 0.05$ vs. the CsA group).

and HCV replication (7,28,32–35). Watashi et al. have found that inhibition of either CypA or CypB expression suppresses HCV replication (12,28). In contrast, Yang et al. have recently revealed that knockdown of CypA, but not of CypB and CypC expression reduces HCV replication (35). Our study suggests that CypA is the principle cyclophilin member for regulation of BKV replication in renal proximal tubular cells.

We demonstrated that knockdown of NFATc3 abrogated BKV TAG expression and reduced the BKV early promoter

activity. In addition, overexpression of either NFATc3 or NFATc4 promoted BKV TAG expression and augmented BKV NCCR early and late promoter activity. Furthermore, NFATc3 and NFATc4 binding to the BKV promoter was verified by the ChIP assay and EMSA. Our results substantiate a critical role of NFAT for BKV TU strain replication. Interestingly, Jordan et al. recently discovered three NFAT binding sites on the promoter of the BKV Dunlop strain (36). They demonstrate that overexpression of NFATc3 or NFATc4 *in Vero* cells augments the viral promoter activity. Mutational analysis reveals that these binding sites are essential for